Nagra
Nationale
Genossenschaft
für die Lagerung
radioaktiver Abfälle

Cédra
Société coopérative
nationale
pour l'entreposage
de déchets radioactifs

Cisra
Società cooperativa
nazionale
per l'immagazzinamento
di scorie radioattive

TECHNICAL REPORT 90-44

STRIPA PROJECT

PREDICTION OF INFLOW INTO THE D-HOLES AT THE STRIPA MINE

J. GEIER
W. DERSHOWITZ
G. SHARP

Golder Associates Inc. Redmond
Washington, USA

APRIL 1990

Parkstrasse 23 5401 Baden / Schweiz Telephon 056 / 20 55 11

Nagra
Nationale
Genossenschaft
für die Lagerung
radioaktiver Abfälle

Cédra
Société coopérative
nationale
pour l'entreposage
de déchets radioactifs

Cisra
Società cooperativa
nazionale
per l'immagazzinamento
di scorie radioattive

TECHNICAL REPORT 90-44

STRIPA PROJECT

PREDICTION OF INFLOW INTO THE D-HOLES AT THE STRIPA MINE

J. GEIER
W. DERSHOWITZ
G. SHARP

APRIL 1990

Golder Associates Inc. Redmond
Washington, USA

Parkstrasse 23 5401 Baden/Schweiz Telephon 056/20 55 11

Der vorliegende Bericht betrifft eine Studie, die für das Stripa-Projekt ausgeführt wurde. Die Autoren haben ihre eigenen Ansichten und Schlussfolgerungen dargestellt. Diese müssen nicht unbedingt mit denjenigen des Auftraggebers übereinstimmen.

Le présent rapport a été préparé pour le projet de Stripa. Les opinions et conclusions présentées sont celles des auteurs et ne correspondent pas nécessairement à ceux du client.

This report concerns a study which was conducted for the Stripa Project. The conclusions and viewpoints presented in the report are those of the authors and do not necessarily coincide with those of the client.

Das Stripa-Projekt ist ein Projekt der Nuklearagentur der OECD. Unter internationaler Beteiligung werden im Rahmen einer 3. Phase dieses Projektes von 1986-1991 Forschungsarbeiten in einem unterirdischen Felslabor in Schweden durchgeführt. Unter Anwendung des in den vorhergehenden Phasen 1 und 2 Gelernten sollen folgende Arbeiten realisiert werden:

- Anwendung verschiedener Felduntersuchungs- und Berechnungsmethoden, um den Wasserfluss und Nuklidtransport in einem unbekannten Felsvolumen des Stripagranites vorherzusagen und anschliessend zu überprüfen
- Evaluation verschiedenster Materialien und Methoden zum Abdichten wasserführender Klüfte im Stripagranit

Seitens der Schweiz beteiligt sich die Nagra an diesen Untersuchungen. Die technischen Berichte aus dem Stripa-Projekt erscheinen gleichzeitig in der NTB-Serie der Nagra.

The Stripa Project is organised as an autonomous project of the Nuclear Energy Agency of the OECD. Over the time period 1986-1991 (Phase 3 of the Project), an international cooperative programme of investigations is being carried out in an underground rock laboratory in Sweden. Building on experience gained in Phases 1 and 2, the following research will be carried out:

- Application of various site characterisation techniques and analysis methods with a view to predicting and validating groundwater flow and nuclide transport in an unexplored volume of Stripa granite
- Verification of the use of different materials and techniques for sealing water-bearing fractures in the Stripa granite

Switzerland is represented in the Stripa Project by Nagra and the Stripa Project technical reports appear in the Nagra NTB series.

Le projet de Stripa est un projet de l'Agence de l'OCDE pour l'Energie Nucléaire. C'est dans le cadre d'une troisième phase de ce projet allant de 1986 à 1991, que des travaux de recherches sont réalisés avec une participation internationale, dans un laboratoire souterrain de Suède. Il s'agit d'effectuer les travaux ci-dessous, en mettant en application ce que l'on a appris au cours des précédentes phases 1 et 2:

- Application de diverses méthodes de recherches sur le terrain et de calcul, pour prévoir puis contrôler l'écoulement de l'eau et le transport des nucléides dans un volume rocheux inconnu du granite de Stripa
- Evaluation des méthodes et des matériaux les plus divers, en vue de colmater des fractures aquifères du granite de Stripa

La Cédra participe à ces recherches pour la Suisse. Les rapports techniques rédigés à propos du projet de Stripa paraissent en même temps dans la série des Rapports Techniques de la Cédra (NTB).

ABSTRACT

Groundwater flow through three-dimensional networks of discrete fractures was modeled to predict the flux into a set of parallel boreholes, as part of the Site Characterization and Validation Project conducted during Phase 3 of the Stripa Project. Influx was predicted from fracture statistics derived from geological, geophysical, and hydrological site characterization data. Individual fractures were treated as probabilistic (random) features, whereas the major fracture zones inferred from geophysics were treated as deterministically located zones of relatively high fracture intensity. The flow predictions were produced by generating multiple, Monte Carlo realizations of the fracture population, and by solving the flow equation for each population using the finite element method. The predictions thus produced are presented in the form of probability distributions for flux. The most likely value for total influx to the boreholes was predicted to be 90 liters/hour, with a 90 % confidence interval extending from 30 to 5700 liters/hour.

Keywords: Site characterization, fracture flow modeling, joint statistics.

RESUME

Dans le cadre du projet de caractérisation et validation réalisé durant la phase 3 du Projet Stripa, on a modélisé la circulation de l'eau dans un réseau à trois dimensions d'un nombre discret de fractures afin de pronostiquer le débit dans un ensemble de forages parallèles. Ces arrivées d'eau ont été prédites sur la base de statistiques des fractures établies sur la base de données provenant de la caractérisation géologique, géophysique et hydrogéologique du site. Les fractures isolées ont été traitées en tant qu'éléments probabilistiques (au hasard), alors que les zones importantes de fractures identifiées par des mesures géophysiques ont été traitées en tant que zones situées en des endroits bien déterminés présentant une intensité relativement élevée de fractures. Les prédictions de débits ont été élaborées en générant de nombreuses populations de fractures par la méthode de Monte Carlo et en résolvant les équations de circulation d'eau pour chaque population en utilisant la méthode des éléments finis. Les prédictions qui en résultent sont présentées sous la forme de probabilités de distribution des débits. La valeur la plus probable prédite pour l'arrivée d'eau totale dans les forages est de 90 litres/heure, avec un niveau de confiance de 90% s'étendant entre 30 et 5700 litres/heure.

Mots clés: caractérisation de site, modélisation de la circulation d'eau dans les fractures, statistiques de joints.

ZUSAMMENFASSUNG

Im Rahmen des Projektes "Site Characterization and Validation" (Charakterisierung und Validierung von Standorten) der Phase III des Stripa-Projekts wurde der Grundwasserfluss durch dreidimensionale Netzwerke von diskreten Klüften modelliert, um den Wasserzufluss in ein System paralleler Bohrlöcher voraussagen zu können. Die Voraussage des Grundwasserzuflusses basierte auf der Kluftstatistik, die aus geologischen, geophysikalischen und hydrogeologischen Standortdaten abgeleitet wurde. Einzelne Klüfte wurden als probabilistische (zufällige) Strukturen behandelt, während die aus Geophysik abgeleiteten grösseren Kluftzonen als deterministisch lokalisierte Zonen mit einer relativ hohen Klüftungsintensität betrachtet wurden. Die Voraussagen des Wasserflusses wurden durch die Erzeugung mehrfacher Monte-Carlo-Realisierungen der Kluftpopulation sowie durch die Lösung der Flussgleichung für jede Population mittels der Methode der Finiten Elemente produziert. Die so erzielten Voraussagen werden als Wahrscheinlichkeitsverteilungen des Grundwasserflusses dargestellt. Der wahrscheinlichste Wert für den gesamten Zufluss in die Bohrlöcher wurde auf 90 Liter/Stunde geschätzt, mit einem 90 % Vertrauensintervall, das von 30 bis 5700 Liter/Stunde reicht.

SUMMARY

This report describes three-dimensional, discrete-fracture flow modeling performed by Golder Associates Inc. for the Simulated Drift Experiment, as part of the Site Characterization and Validation Project conducted during Phase 3 of the Stripa Project. The objective of this exercise was to predict groundwater flow into a "simulated drift" consisting of six parallel boreholes, which were intended to represent a drift (tunnel) along the length of the boreholes, having a perimeter defined by the locations of the boreholes.

A 200m x 200m x 200m volume of rock around the simulated drift was modeled as a population of discrete fractures. A 20m-diameter cylinder around the simulated drift was modeled using a detailed fracture population, while the remaining, outer region of the 200m x 200m x 200m cube was modeled with a "coarse" population of larger fractures.

Individual fractures were treated as probabilistic features, with location and other properties described by probability distributions. Fracture statistics were derived from site-characterization data that included core logs, scanline surveys, and results of single-hole and cross-hole hydrological tests. Forward modeling was used in this derivation to match the field data while explicitly accounting for many of the biases arising from site characterization methods. Conductive fracture frequency and transmissivity distributions were estimated from fixed-interval-length packer tests. Mean fracture storativity was estimated from cross-hole hydrological tests. Fractures were treated as nearly circular polygons, and the fracture radius distributions were estimated from trace-length data.

Major features that were identified during site characterization by geophysical methods were included in the model as zones of elevated fracture intensity. Fracture intensities in these zones were estimated from core log data. Transmissivity distributions for the outer region of the model were calibrated using the model to predict fluxes into older drifts and boreholes, for which flux measurements were available.

The flow into the simulated drift was predicted by generating multiple, Monte Carlo realizations of the fracture population using the FracMan Discrete Fracture Simulation Model (Golder Associates, 1989b). For each Monte Carlo realization, a finite element mesh was produced and the flow equation was solved by the finite element program MAFIC (Golder Associates, 1989c).

The predictions produced in this modeling exercise are in the form of probability distributions for flux. The most likely value for total influx to the simulated drift was predicted to be 90 liters/hour with a 90% confidence interval extending from 30 to 5700 liters/hour. A prediction is given of the distribution of influx along the length of the simulated drift. 75% of the inflow is predicted to occur where the major features intersect the simulated drift.

TABLE OF CONTENTS

TABLE OF CONTENTS (Continued)

Page

LIST OF FIGURES

1 INTRODUCTION

1.1 SCOPE

The purpose of the Site Characterization and Validation (SCV) Project is to assess methods for characterizing a volume of rock for use as a repository. The program of work addresses the problem of validating the techniques used in site characterization. The program aims to predict groundwater flow in a specific volume of rock, and to compare the predicted flow with data from field measurements. In this program the distribution of water flow into a drift will be predicted, the drift will be excavated, and the inflows to the drift will be measured and compared with the predicted inflows.

The site for the SCV Project is a volume of rock between the 340- and 410-meter levels of the Stripa mine, located as shown in Figure 1-1. The project comprises two cycles of site characterization and validation (comparison of observations with predictions), which are to be carried out in five stages of work:

I. Preliminary site characterization

II. Preliminary predictions

III. Preliminary validation and detailed characterization

IV. Detailed predictions

V. Detailed validation

Stage I consisted of data collection using a variety of geological, geophysical, and hydrological methods. In Stage II these data were used to formulate a prediction of the geometrical characteristics of the fractures within the site. For Stage III, which is underway at the time of this report, two sets of boreholes referred to as the C- and D- holes have been drilled and are being used for detailed characterization exercises. The C-holes are being used mainly for crosshole hydrological and geophysical testing. The D-holes, which run parallel to and slightly inside of the perimeter of the planned validation drift, are being used in the Simulated Drift Experiment (SDE). In this experiment, the fluxes into the D-holes are to be predicted by fracture flow modeling, using the results from Stages I and II as input to the models. These predictions will be compared with the inflows measured during Stage III. Stage IV will be a detailed prediction of the fluxes into the actual validation drift, using the results of Stage III to refine the models used. In Stage V,

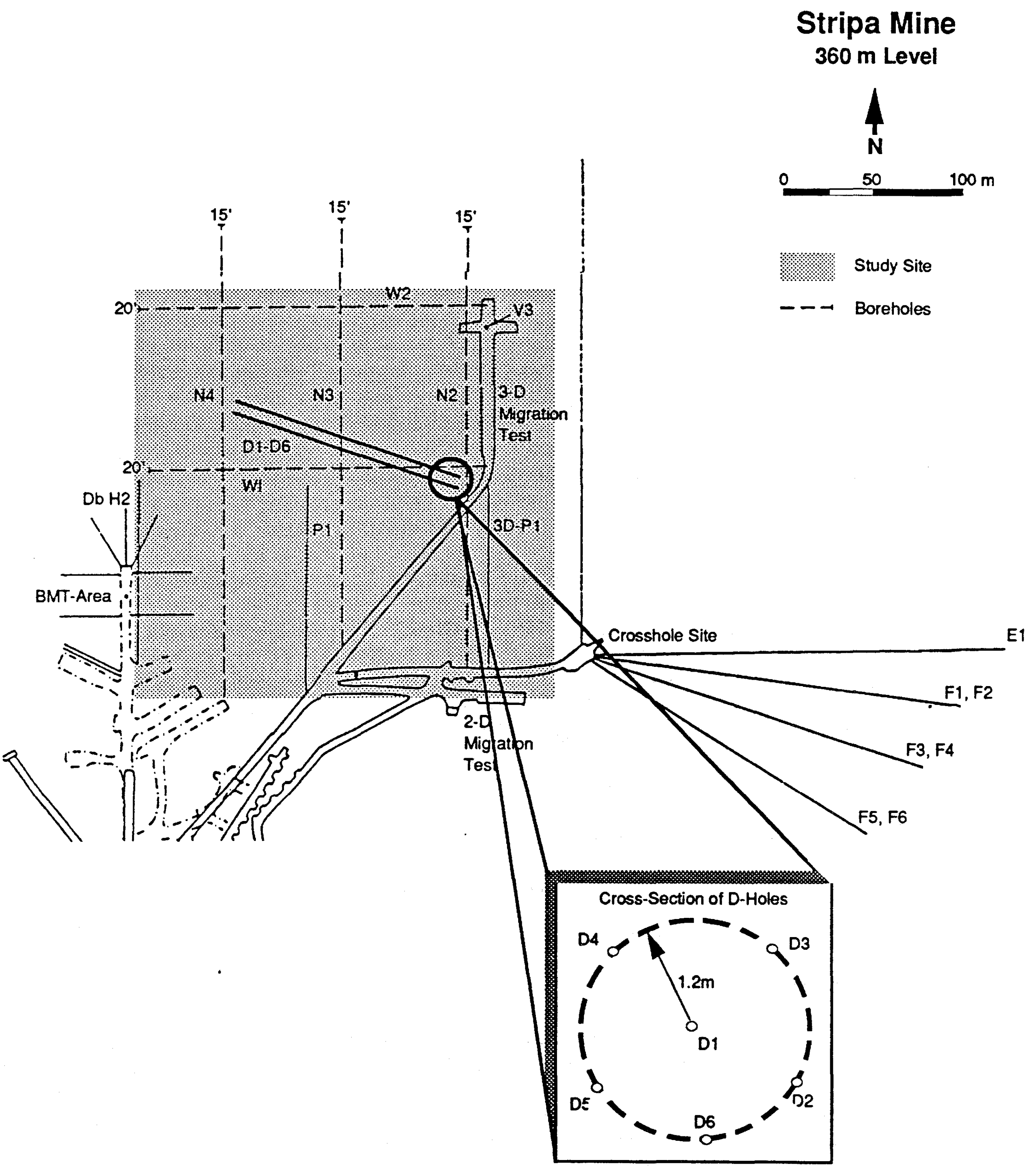

Sources of data for simulated drift experiment prediction

- Borehole N2, N3, N4, W2, W1,
- Mapping of 3-D Migration Test and access drifts

Simulated Drift Experiment consists of boreholes D1, D2, D3, D4, D5, and D6

FIGURE **1-1**

LOCATION OF THE STUDY SITE AND STAGE 1 BOREHOLES

STRIPA

PROJECT NO. 883-1313.031 DWG. NO. 20136 DATE 9/13/89 DRAWN CB APPROVED JG the drift will be excavated, and the influxes to the drift will be measured and compared with the predicted fluxes.

This report describes discrete fracture flow modeling performed by Golder Associates for the Simulated Drift Experiment (SDE). The goal of this work was to demonstrate the practical application of the discrete fracture flow modeling approach, by predicting the flow into a set of parallel boreholes using only data from boreholes and drift walls characterized during previous phases (Figure 1-1). Data from the site characterization program was used to formulate a combined deterministic/statistical model of fractures in the rock around the experimental drift. This model was used to predict the groundwater response to the simulated drift experiment.

Firstly, a probabilistic prediction was produced of the distribution of steady-state flux along the length of each of the D-holes. This prediction is analogous to the prediction of the fluxes to individual canisters emplaced along a borehole, an important problem in repository performance assessment.

Secondly, the total, steady-state flux into all of the boreholes was predicted by combining the predicted distributions of flux along the lengths of all D-holes. This prediction was a minimal objective of the SDE modeling study. It serves as an estimate of the flux into a drift, the boundary of which would be defined by the D-holes. This is analogous to a prediction of the total flux into a repository shaft or tunnel.

1.2 PHILOSOPHY OF APPROACH

Groundwater flow at the SCV site is expected to be primarily through fractures, due to the low permeability of unfractured Stripa granite. A semi-statistical model was chosen that combined deterministic information on fracture zone location with statistical information on fracture properties. The hydrologically conductive fractures at the site were modeled as a stochastic population of discrete fractures, with stationary statistics for all fracture properties except location. Fracture locations were assumed to be randomly distributed in a three-dimensional field, with elevated intensity in the fracture zones that were identified by geophysical methods. Figure 1-2 shows the locations of fracture zones that were inferred from seismic velocity tomography and seismic reflection profiles by Ollson et al. (1989).

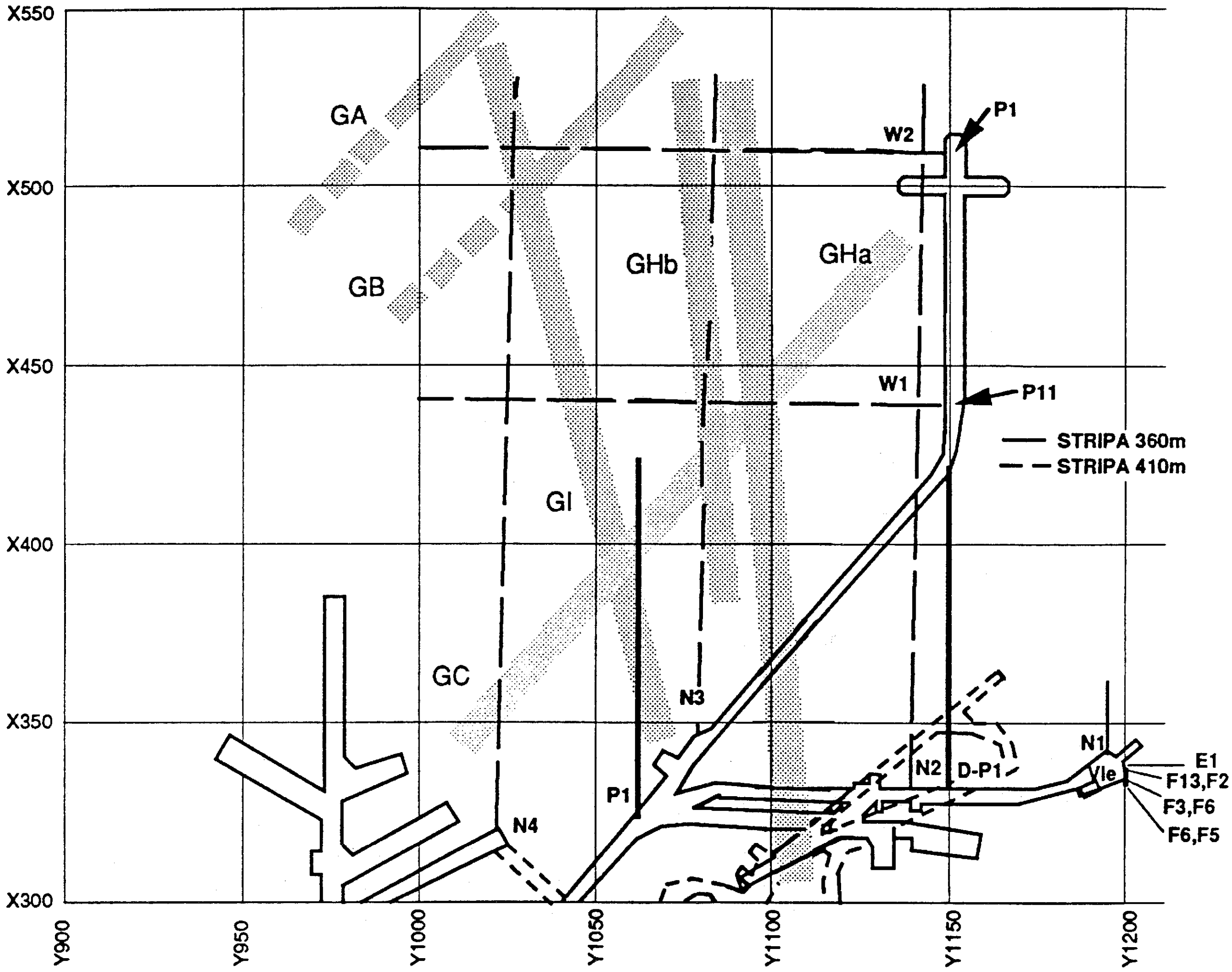

Key:

Location of Fracture Zones Inferred from Geophysics by Olsson et al., 1989.

FIGURE **1-2A**

LOCATION OF MAJOR AND MINOR FEATURES AT THE SCV SITE 360 LEVEL

STRIPA

883-1313.031 DWG. NO. 20137 DATE 8/16/90 DRAWN DC

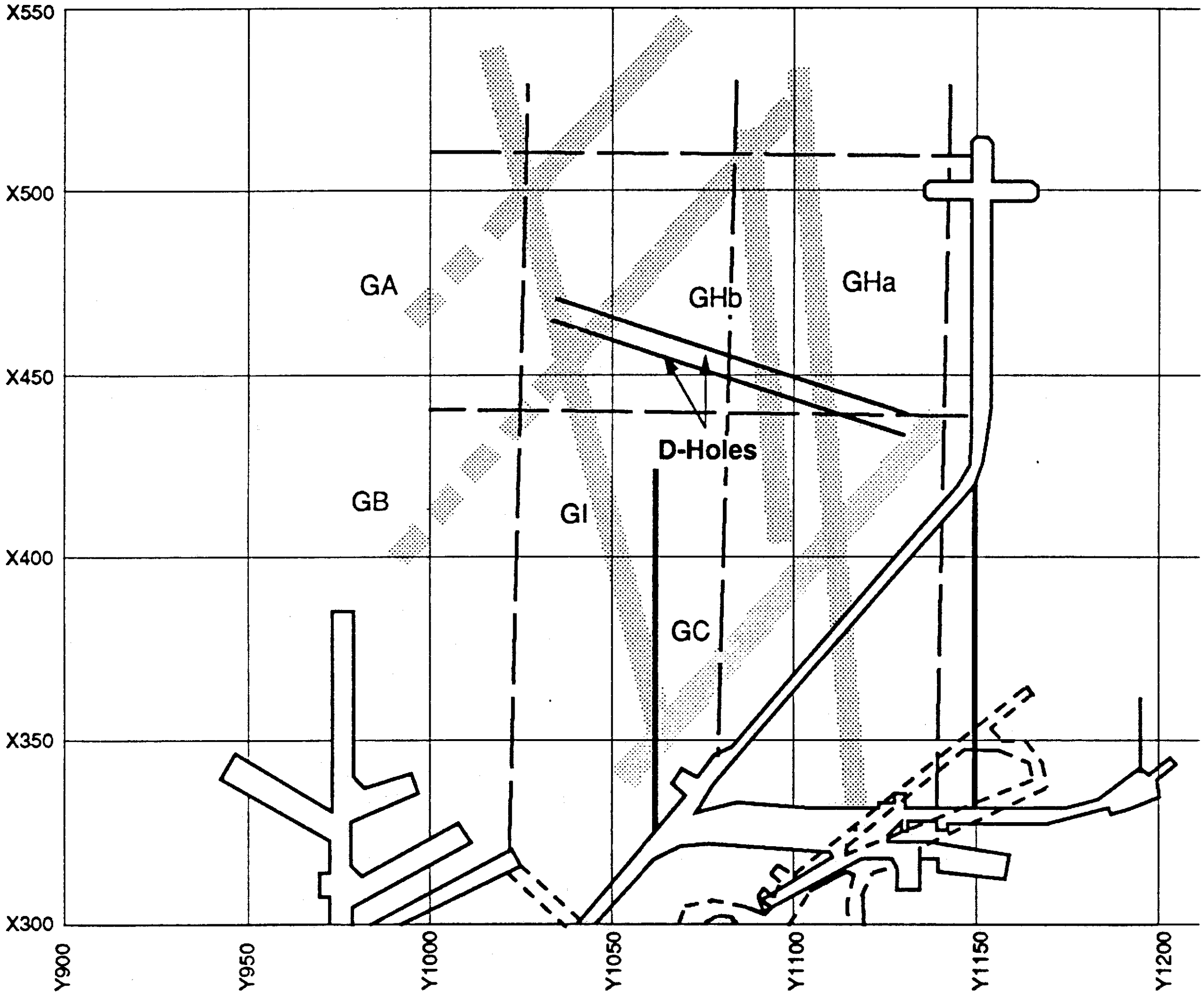

Key:

Location of Fracture Zones Inferred from Geophysics by Olsson et al., 1989.

FIGURE **1-2B**
LOCATION OF MAJOR AND MINOR FEATURES AT THE SCV SITE 385M LEVEL
STRIPA

PROJECT NO. 883-1313.220 DWG. NO. 00000 DATE 4/10/90 DRAWN CB

The discrete fracture approach provides a physically realistic model for predicting flux in a volume of fractured rock with irregular connectivity features. Observations of crosshole responses by Olsson et al. (1989) demonstrated the existence of anomalous connections between the N- and W-boreholes on the 360 m level of the SCV site (Figure 1-1). In this study, pressures were measured in packed-off zones of the W1, N3, and N4 holes while the W2 hole was uncapped for periods of 55 to 99 minutes. Figure 1-3 shows the responses in terms of the apparent speed at which the pressure perturbations in the W2 hole propagated to zones in the other holes. In some cases, the zones responding to the pressure disturbance are associated with the major features identified by Olsson et al. However, some zones that are intersected by the major features show no response, and another zone (in N4) shows a response although it is not intersected by a major feature. Anomalous connections such as these cannot be modeled by continuum methods. The discrete fracture approach allows simulation of this type of behavior.

Most fracture properties -- location, size, orientation, transmissivity, and storativity -- were treated as stochastic variables. Fracture intensity was treated as a deterministic variable, with higher values in zones that were believed to have higher intensities based on the results of Olsson et al. In a highly fractured rock mass such as the SCV site, individual fractures and their properties cannot be measured remotely. Hence a fully deterministic model of the site is not possible. However, the information that is available concerning the locations, orientations, and extents of major fracture zones can be incorporated into the model by specifying fracture intensities (i.e., the total fracture area per unit volume of rock) deterministically. This approach produces deterministically-located zones of stochastic fractures. The probability distributions for the geometric variables were inferred from core and scanline data. Probability distributions for the hydrological properties were obtained from the results of wellbore tests. The collection of fractures that exists within the SCV site is viewed as being a particular realization of these distributions.

The modeling region defined for this exercise is a 200 x 200 x 200 meter cube surrounding the SCV site. This region was chosen to include the important hydrological features of the mine in the vicinity of the SCV site. The modeling region consists of an inner, cylindrical subregion in which the conductive fracture population was simulated in nearly full detail, and an outer subregion in which a sparser fracture population was used. This scheme was adopted instead of modeling the entire region in full detail, since limitations of

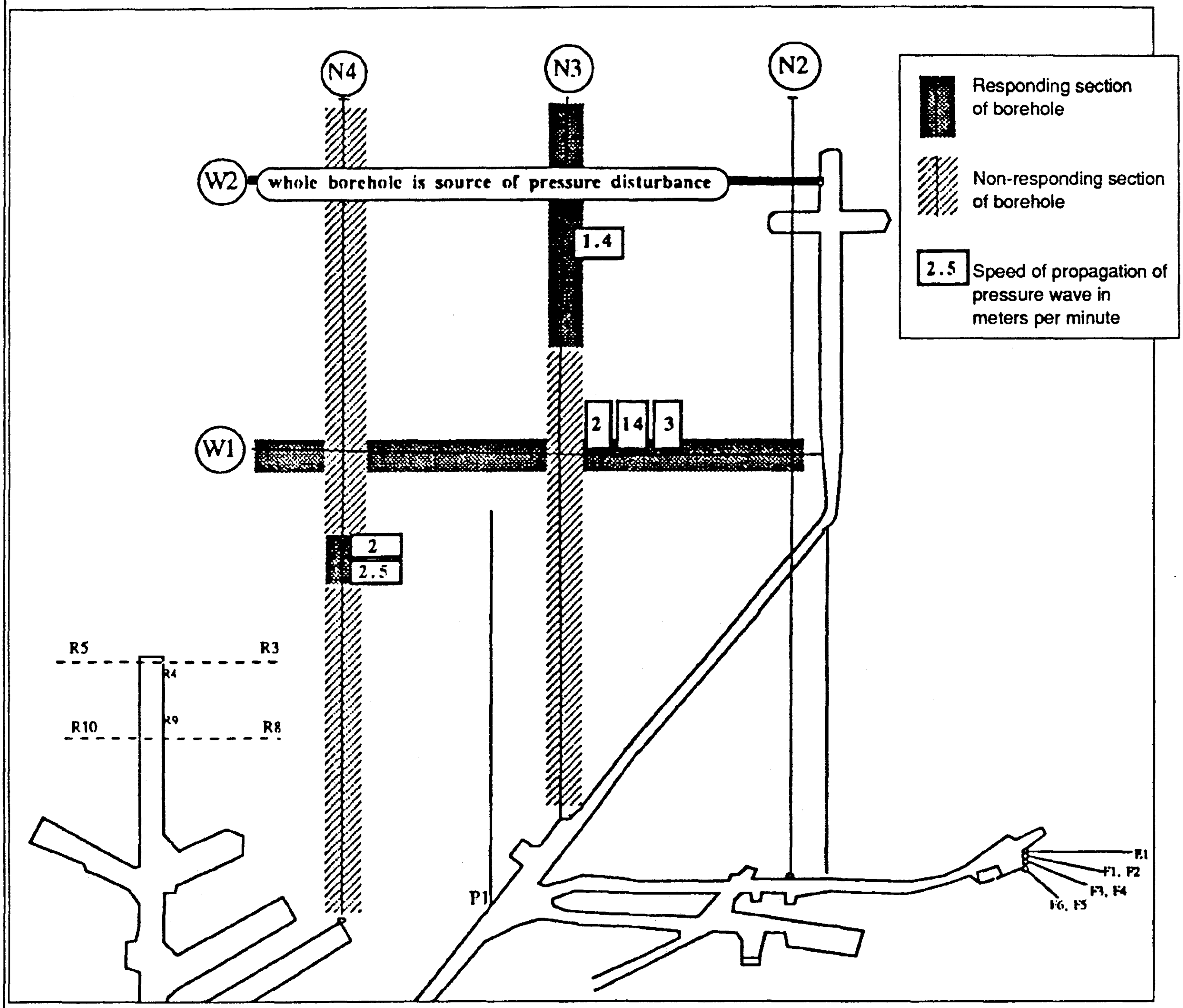

FIGURE **1-3**

RESPONSES OBSERVED IN ADJACENT BOREHOLES DUE TO SHORT-TERM DISTURBANCES IN BOREHOLE W-2

STRIPA

PROJECT NO. 883-1313.031 DWG. NO. 20135 DATE 9/13/89 DRAWN CB

computer speed constrained the number of fractures that could be handled in a Monte Carlo analysis. All major mine openings and all boreholes within the 200-meter cube were included in the model geometry.

The inner subregion was defined as a cylindrical region 20 meters in diameter around the D-holes (Figure 1-4). This subregion was modeled using a truncated fracture size distribution such that all conductive fractures of radius greater than 1m were included in the model. Given computational constraints which prevented the use of full-intensity statistics over a larger region, this detailed inner subregion provided the most realistic model possible for predicting the distributions of flux into the D-holes

The outer subregion was modeled with a fracture population having the same basic size distributions as the fractures in the inner region, but using a higher cutoff so that only the fractures with radius larger than 5m were modeled. This approach was taken due to computational constraints, in order to reduce the total number of fractures in the outer region. The outer region was needed to avoid excessively influential boundary conditions on the periphery of the detailed model. In a real fracture network, a highly conductive path would rapidly drain the fractures at the beginning of the path, reducing the head gradient along the path and hence the steady-state flowrate (Figure 1-5). Imposing a constant head condition on the boundary of the detailed, inner subregion would have resulted in artificially high head gradients and flowrates through the more highly conductive pathways.

A sparse fracture network was used for the outer subregion rather than a stochastic continuum, because a stochastic continuum with an equivalent distribution of permeabilities would have a higher degree of connection than the real fracture network.

The effects of stress on flow through the fractures were not accounted for in this study. Although excavation disturbance and stress concentration around a drift might significantly affect the flux into the drift, this effect would be much smaller for the simulated drift experiment, which is based upon boreholes. The zone of stress concentration and excavation disturbance for a borehole is much smaller than for a drift. An empirical, log-linear relationship between the stress normal to the plane of a fracture and the transmissivity of the fracture in Stripa quartz monzonite has been determined from the laboratory data of Gale et al. (1987) by Golder Associates Inc. (1988a) as:

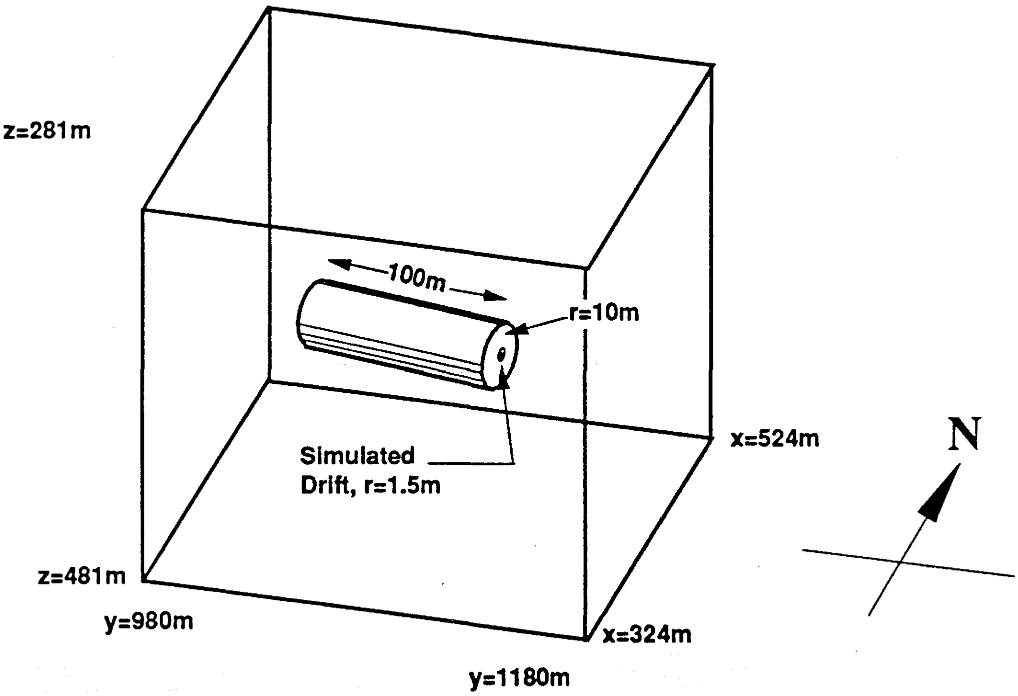

FIGURE **1-4**
BOUNDARIES OF INNER AND OUTER SUBREGIONS
STRIPA

PROJECT NO. 883-1313.031 DWG. NO. 20009 DATE 8/16/89 DRAWN CB APPROVED BD

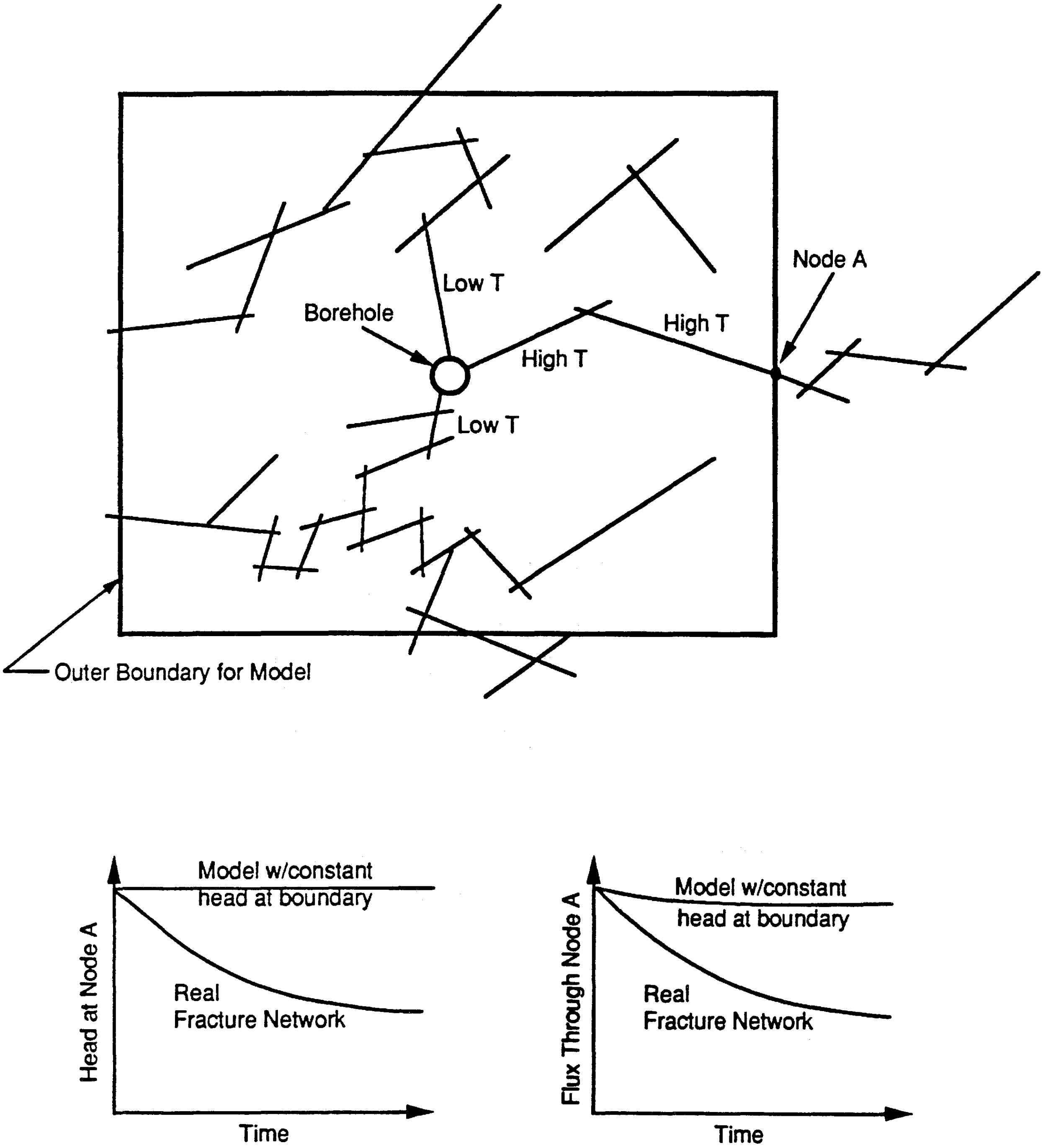

FIGURE **1-5**
BEHAVIOR OF A HIGHLY TRANSMISSIVE PATHWAY INTO A BOREHOLE; COMPARISON BETWEEN A MODELED NETWORK WITH A CONSTANT HEAD BOUNDARY AND A FRACTURE NETWORK WITH BOUNDARY CONDITIONS EFFECTIVELY AT INFINITY

STRIPA

$$T = T_{1MPa}\ \sigma^n \tag{1-1}$$

where:

T = transmissivity

T_{1MPa} = T at 1 MPa normal stress

σ = normal stress

n = change in T per log cycle of σ

The log-slope of this relationship of transmissivity to normal stress was found to be approximately -0.63 (Golder Associates Inc., 1988). The change in stress around an opening of circular cross section can be estimated from the elastic, plane-strain solution for the stress around a circular hole in an infinite sheet (Jaeger and Cook, 1977):

$$2\sigma_r = (p_1 + p_2)(1 - \rho^2) + (p_1 - p_2)(1 - 4\rho^2 + 3\rho^4)\cos 2\theta \tag{1-2}$$

$$2\sigma_\theta = (p_1 + p_2)(1 + \rho^2) - (p_1 - p_2)(1 + 3\rho^4)\sin 2\theta \tag{1-3}$$

where:

σ_r = radial stress

σ_θ = tangential stress

p_1, p_2 = maximum and minimum far-field stresses

ρ = R/r

r = radial distance from the center of the hole

R = radius of the hole

θ = angle from the p_2 direction

Figure 1-6 shows the range of transmissivity stress effects predicted from Equations 1-1 and 1-2 for fractures oriented radially with respect to a 1.5m radius drift and a 0.05m radius borehole. Since the effects of stress on the transmissivity of fractures around a borehole are negligible beyond a distance of about 0.2m, which is less than the mean fracture radius, stress effects were not taken into account in the simulations for the simulated drift. For the simulations of the validation drift, stress and excavation effects will be incorporated.

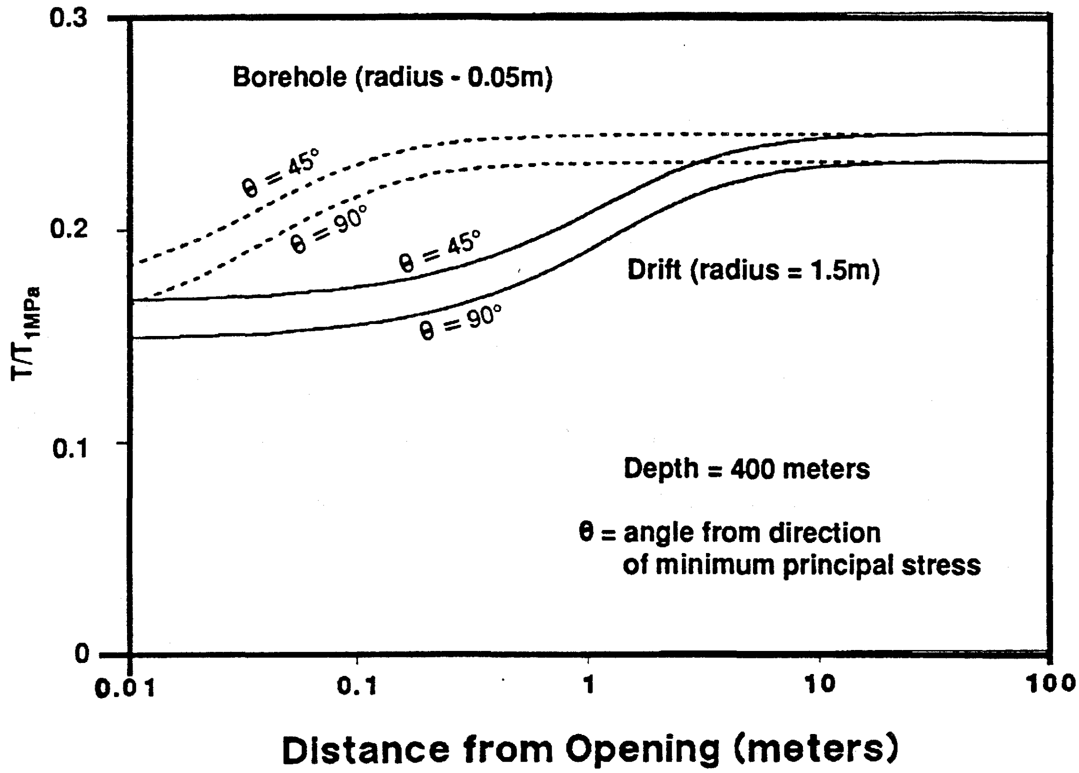

FIGURE **1-6**

EFFECTS OF STRESS ON TRANSMISSIVITY OF RADIALLY ORIENTED FRACTURES

STRIPA

883-1313.031 DWG. NO. 20137 DATE 8/16/90 DRAWN DC

2 DESCRIPTION OF THE MODEL

2.1 MINE GEOMETRY

The Stripa mine consists of a complex network of shafts, stopes, and tunnels. The mine is the deepest sink in the region, and by virtue of its age and excavated volume it exerts a profound influence on the regional groundwater flow, to the extent that some regional flows appear to have been reversed by the presence of the mine (Olsson et al., 1989). As stated by Olsson et al., "[i]ts effects are ... seen at large distances from the mine and the presence of the fracture zones ensures that flow directions are extremely variable on a local scale." A mine opening may have a very strong influence on the flow patterns, or it may have almost no influence, depending on whether it intercepts a major fracture flow path or not. Since a distance of ten or twenty meters could determine whether or not an opening intersects a major flow path, an effort was made to represent all mine features as precisely as possible.

Only a relatively small number of the mine drifts and shafts protrude into the 200-meter cubical modeling region. All of these have been included in the model except for a few short, spur drifts on the 335-meter level, and other drifts that are within a few meters of more salient, approximately parallel drifts. Figure 2-1 shows a three-dimensional view of the modeling region, showing all drifts, shafts, and boreholes. This model geometry is a very close representation of the actual mine geometry within the modeling region. Table 2-1 gives the coordinates of all drifts, shafts, and boreholes that were included in the model, in terms of the system of coordinates used in the FracMan package. The right-handed coordinate system used has its positive x axis pointing due south, the y axis pointing due east, and the z axis pointing in the upward direction, with the origin of the system lying at x = 424 m, y = 1080 m and depth = 381 m, in mine coordinates. The coordinates given in Table 2-1 were adapted from Olsson et al., 1989.

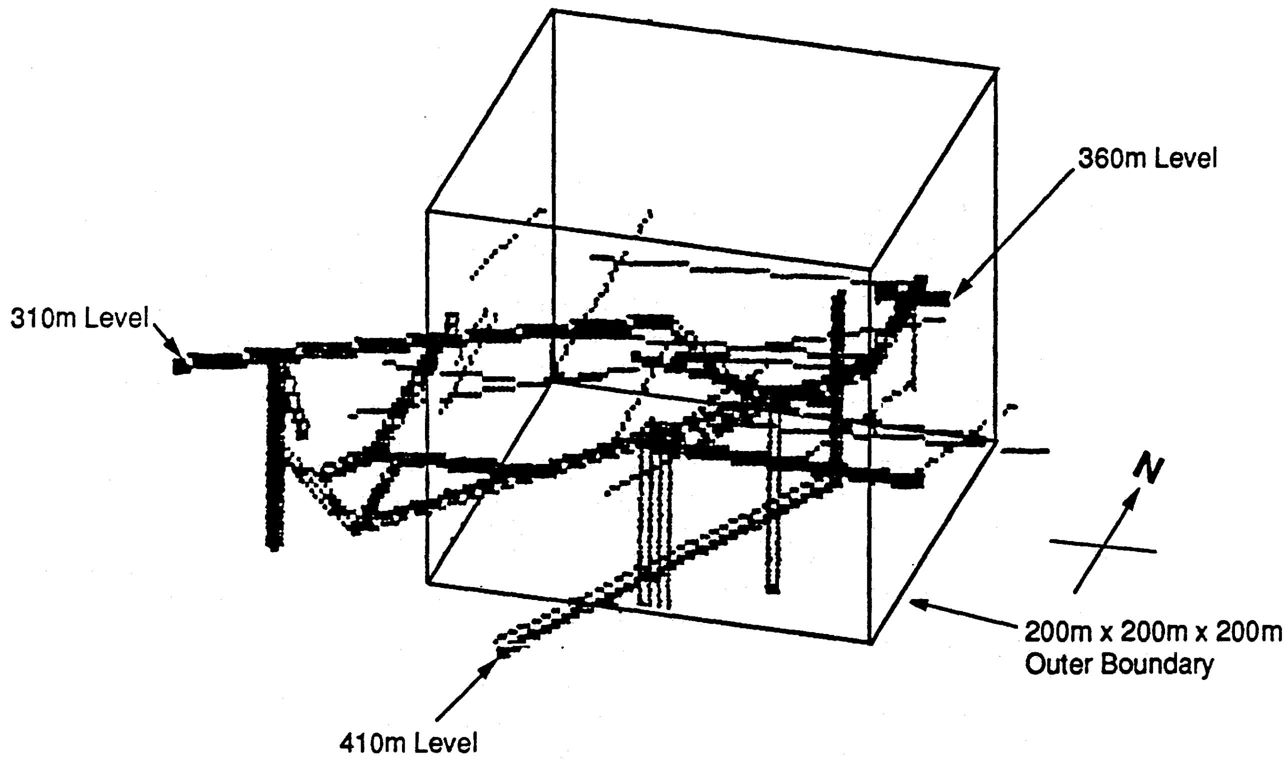

FIGURE **2-1**

REGION MODELED TO PREDICT FLUX INTO THE D-HOLES

STRIPA

PROJECT NO. 883-1313.031 DWG. NO. 20010 DATE 8/16/89 DRAWN DT APPROVED BD

Table 2-1 Coordinates of Mine Openings and Boreholes (BH)

Feature Name	x (m)	y (m)	z (m)	Trend (degrees)	Plunge (degrees)	Length (m)	Radius (m)
Mine Openings							
Shaft 1	9	60	71	0	90	100	2
Shaft 2	114	60	71	0	90	100	2
Shaft 3	134	-160	71	0	90	100	2
Drift 1	134	-160	71	156	0	72	2
Drift 2	154	-200	71	63	0	219	2
Drift 3	54	-5	71	137	0	88	2
Drift 4	174	-105	51	0	0	130	2
Drift 5	174	-105	51	52	18.6	89	2
Drift 6	174	-105	51	210	0	30	2
Drift 7	200	-105	26	320	0	86	2
Drift 8	200	-105	26	0	0	61	2
Drift 9	200	-105	26	41	0	267	2
Drift 10	89	-10	26	90	0	130	2
Drift 11	-1	70	26	0	0	90	2
Drift 12	-76	55	26	90	0	30	2
Drift 13	200	-40	-29	19	0	91	2
Boreholes							
BH 96	62	10	71	85	0	155	0.05
BH C1	-14.5	67	24.8	270	38	150	0.05
BH C2	-18.5	67.1	24.7	305	40	150	0.05

Table 2-1 Coordinates of Mine Openings and Boreholes (BH) (Cont.)

Feature Name	x (m)	y (m)	z (m)	Trend (degrees)	Plunge (degrees)	Length (m)	Radius (m)
BH C3	-8.9	67.6	25.1	287	14	100	0.05
BH D1	-15.1	47.9	-2.3	287	3	100	0.05
BH D2	-13.9	47.7	-2.6	287	3	100	0.05
BH D3	-14.3	48.1	-1.3	287	3	100	0.05
BH D4	-15.7	48.3	-1.3	287	3	100	0.05
BH D5	-16.1	48.4	-2.6	287	3	100	0.05
BH D6	-14.9	48.3	-3.4	287	3	100	0.05
DBH2	84	-100	46	0	0	90	0.05
HG (composite)	39	-105	46	0	0	50	0.05
N1	84	115	26	0.4	18.0	170	0.05
N2	90.7	59.2	24.3	1.1	17.8	207	0.05
N3	76.6	-0.9	24.1	0.7	18.1	189	0.05
N4	102.9	-56.9	36	0	0	205	0.05
P1	99	-20	26	0	0	100	0.05
R (composite)	51	-135	26	90	0	60	0.05
V3	-78.9	69.7	24.5	0	89.4	50	0.05
W1	-16.0	-66.8	24.9	270.7	4.6	147	0.05
W2	-86.0	67.4	25.7	270.5	4.2	147	0.05

2.2 BOUNDARY CONDITIONS

Significant gradients in total head exist within the modeling region, due to the drawdown around the mine. This condition is represented in the model by imposing temporally fixed, spatially varying heads on each face of the 200-meter cube. A linear variation of head with respect to the x, y, and z axes was used, with the general mathematical form:

$$H = H_x x + H_y y + H_z z + H_o \qquad (2\text{-}1)$$

Table 2-2 gives the coefficients H_x, H_y, H_z, and H_o for each of the sides of the outer boundary. The coefficients H_x, H_y, and H_o were estimated from the head measurement of Carlsten et al. (1988) on the 360-m level, by taking linear approximations to the smoothed head values fitted by Golder Associates (1988a), along each side of the modeling region. The H_z coefficient is based upon the assumption of hydrostatic gradient.

Table 2-2. Boundary condition coefficients for outer boundary.

Face	H_x	H_y	H_z	H_o (m)
East	-0.053	0	1.0	192.4
West	-0.001	0	1.0	182.6
North	0	0.074	1.0	190.1
South	0	0.023	1.0	184.9
Top	-0.026	0.049	1.0	187.5
Bottom	-0.026	0.049	1.0	187.5

Drifts and shafts were assigned temporally fixed, spatially varying heads equal to the elevation of each point on their walls. This boundary condition was used because the openings are kept drained by pumping at the bottom of the mine. The same type of boundary condition was used for the D-holes, because the holes will be drained during the inflow measurement stage. Table 2-3 gives the coefficients H_x, H_y, H_z, and H_o for the drifts and shafts.

Table 2-3. Boundary condition coefficients for drifts and shafts.

Opening	H_x	H_y	H_z	H_o (m)
(All)	0	0	1.0	0

The other boreholes within the region of the model will be capped during the simulated drift experiment. These capped boreholes will act as linear flow paths, with flow out of some fractures and into others such that the net flux into each borehole is zero. This situation was modeled in MAFIC by using a group-flux-boundary condition for each of the boreholes, and fixing the net flux into each borehole at zero. The group-flux boundary condition as implemented in MAFIC allows the specification of the net flux across a boundary while maintaining head equilibrium among the fracture nodes on the boundary.

2.3 COMPUTER PROGRAMS USED IN MODELING

Discrete fracture modeling was performed using the FracMan Discrete Fracture Network Modeling package (Golder Associates Inc., 1988b) and the finite element program MAFIC (Golder Associates Inc., 1988c). The FracMan package was used to generate discrete fracture networks, to simulate site characterization methods, to define boundary geometries and boundary conditions, and to generate finite element meshes from the fracture networks. MAFIC is used to solve the flow equations for the finite element meshes.

FracMan is an interactive, discrete fracture modeling package consisting of the two principle programs FracWorks and MeshMaker, and several supporting utility programs. The program FracWorks is used to generate and display fractures in three-dimensional space, and to simulate fracture sampling methods used in site characterization programs, such as core logging (Figure 2-2) and scanline surveys (Figure 2-3). FracWorks can generate fractures deterministically, stochastically, or by a combined deterministic-stochastic process. In the present modeling study, FracWorks was first used to refine the dataset for fracture properties, by using the sampling features to simulate data collection procedures and deduce fracture properties while developing the dataset for the final model. Once the dataset was established, FracWorks was used to generate fractures according to the combined deterministic-probabilistic conceptual model.

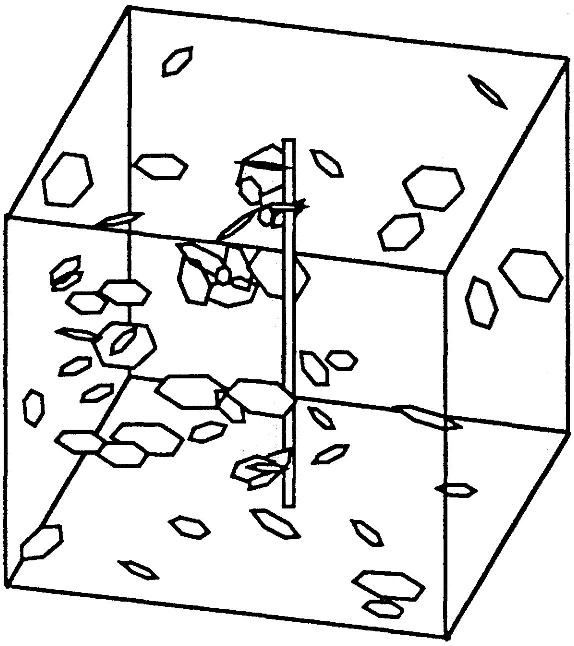

(a) Borehole in 3 - D Fracture Population
(Note: Fracture intensity less than actual intensity)

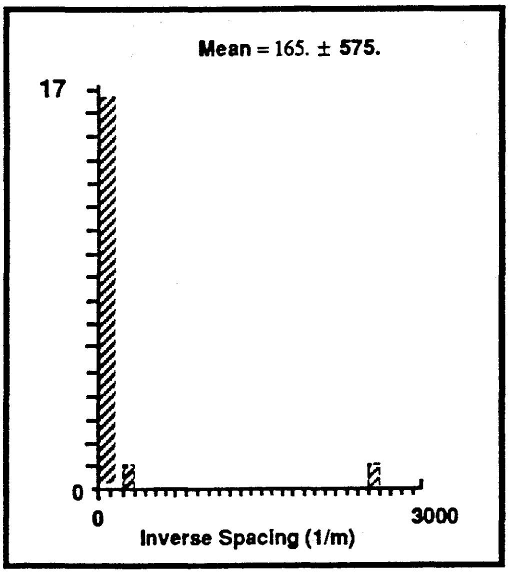

(b) Fracture Spacing

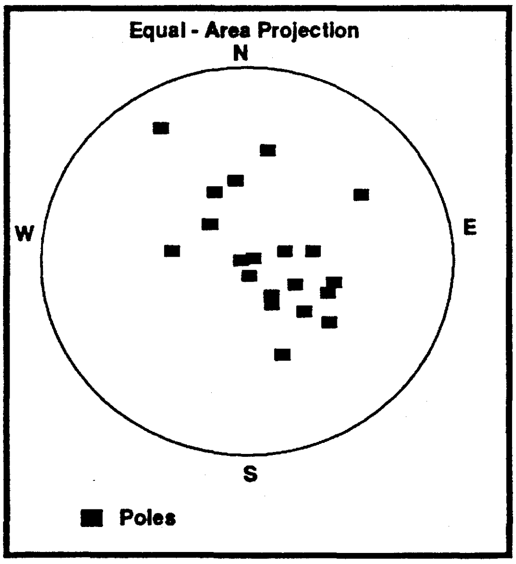

(c) Orientations

FIGURE **2-2**

SIMULATED CORE LOGGING USING FRACMAN

STRIPA

883-1313.031 DWG. NO. 20007 DATE 8/16/90 DRAWN DC

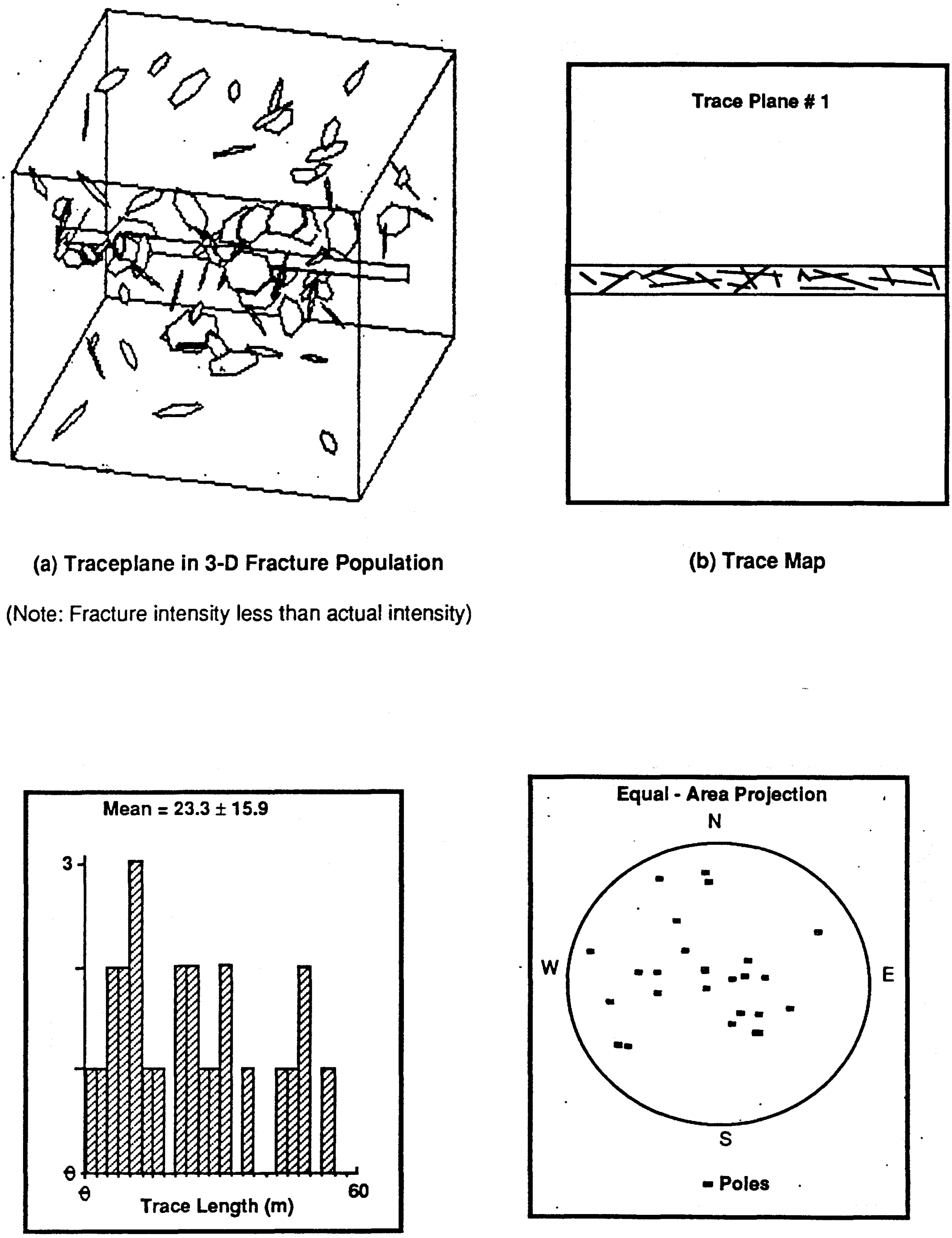

(a) Traceplane in 3-D Fracture Population

(Note: Fracture intensity less than actual intensity)

(b) Trace Map

(c) Trace Length

(d) Orientations

FIGURE **2-3**
SIMULATED TRACEPLANE SURVEY USING FRACMAN
STRIPA

PROJECT NO. 883-1313.031 DWG. NO. 20008 DATE 8/16/89 DRAWN DT APPROVED BD

The FracMan program MeshMaker was used to define boundary geometries and assign boundary conditions to the model prior to forming finite-element meshes. For the large fracture populations used in the model, the VAX-based FracMan utility program MeshMonster was used to generate the finite element meshes, since the PC-based MeshMaker program is prohibitively slow in forming meshes from populations of more than a few hundred fractures.

MAFIC reads the mesh files created by MeshMaker or MeshMonster, optimizes nodal numbering, assembles the finite element equations for transient, saturated fracture flow, and solves the finite element problem using either direct or iterative matrix solution techniques. The MAFIC matrix flow and transport modeling options were not utilized in this modeling study.

In addition to these programs, three other programs were used in developing the dataset for the model: Lotus 1-2-3 Release 2.0 (Lotus Development Corporation, 1985), @RISK Version 1.5 (Palisade Corporation, 1989), and ISIS (Golder Associates Inc., 1989). Lotus 1-2-3 and @RISK are commercially available software. Lotus 1-2-3 is a spreadsheet package, and @RISK is an auxiliary program that adds Monte Carlo simulation capabilities to Lotus spreadsheets. ISIS (Iterative Set Identification System) is a program that identifies fracture sets on the basis of orientation.

3 DERIVATION OF FRACTURE PARAMETERS

3.1 PHILOSOPHY

The site characterization activities for the simulated drift experiment provided a data set that is comparatively rich in information. Scanlines in tunnels at the boundary of the site afforded information on fracture radius that would not have been available from borehole logs alone. Seismic and radar tomography indicated the locations of major fracture zones away from boreholes and tunnels. Packer tests gave estimates of the hydrologic properties of the fractures. Given this relative wealth of data, the first task in this modeling study was to compile the most realistic description possible of the fracture population.

A fundamental premise of this analysis was that only a fraction of the fractures present in the rock are significantly conductive. This is evident from packer tests in zones that showed no appreciable conductivity, although core logs showed multiple fractures in those zones. By modeling only the conductive fractures, a realistic prediction can be obtained with considerably less computational effort than would be required to model all of the fractures. For this approach it was necessary to determine the conductive fracture intensity:

P_{32c} = total area of conductive fractures in a unit volume of rock

rather than the total fracture intensity:

P_{32} = total area of fractures in a unit volume of rock,

using the notation of Dershowitz (1984).

The P_{32c} intensity for a given fracture set can be found from the conductive fracture frequencies f_c in a group of boreholes, by using FracMan simulated borehole sampling to determine the net effects of bias due to the particular combination of fracture orientations, borehole orientations, and borehole lengths. The values of f_c and fracture transmissivity statistics that give the best match to fixed-interval-length (FIL) hydrologic tests can be determined by trial-and-error using simulated sampling.

Fracture pole orientation distributions were determined from borehole and scanline data, which were combined after correcting for orientation bias, and were analyzed as if both types of data represented line samples. This introduced an error in that the scanline data did not represent a true line sample, since fracture traces longer than two meters had been mapped even if they did not cross the scanlines (Gale and Stråhle, 1988). However, since the larger fractures constituted only a small portion of the mapped fracture population, the error in orientation statistics that might arise from this inconsistency was thought to be insignificant.

Fracture-size distributions (equivalent fracture radius) were determined by forward modeling to match trace-length statistics, using @RISK to simulate the effects of sampling bias. The fracture size distributions were adjusted by trial-and-error to obtain a match to the trace length statistics corrected for truncation and censoring by Gale and Stråhle (1988). An alternative approach using **FracMan** to simulate truncation, censoring, and sampling-bias effects was not used because the available data had already been corrected for truncation, and because the present version of **FracMan** is designed primarily for statistical comparison of trace-length sampling with fitted distributional forms, not raw tracelength data.

This derivation of fracture parameters was implicitly based on the assumption of homogeneous, stationary statistics for the fractures within the modeling region. The possibility that the statistics describing the fracture population may vary in space was not taken into account. This determination is also based upon the assumption that characteristics of the fractures such as orientation and transmissivity are independently distributed. The effects on flow of any correlations among fracture properties may be profound, but methods of determining such correlations from field data are not well developed.

3.2 ORIENTATION

Fracture pole orientation distributions were determined from borehole and scanline data using the Golder Associates program ISIS, which identifies sets of fractures according to orientation by an iterative process. A modified-Terzhagi correction (adapted from Terzaghi, 1965) was applied to the data for each borehole and each scanline separately before running ISIS, in order to compensate for sampling bias due to borehole orientation. For each fracture record in the original dataset, N records were included in the Terzaghi-corrected dataset, where:

$$N = \min\{1/[3\cos\beta],\ 7\}, \tag{3-1}$$

where:

β = the angle between the normal to the fracture plane and the borehole or scanline direction.

A maximum value of N = 7 was set to avoid excessively strong correction for fractures nearly parallel to the boreholes. ISIS requires as input a file containing fracture orientation data. The data analyst specifies the number of fracture sets to search for, and an adjustable damping parameter, d, that controls the stability of the set-identification algorithm. The analyst may let ISIS search automatically for fracture sets, or alternatively the analyst may guide the search by specifying initial parameters of Fisher distributions for each set.

For each fracture orientation, ISIS calculates the value of the Fisher distribution probability density function (p.d.f.):

$$f(\phi',\theta') = K \sin\phi' e^{K\cos\phi'}/4\pi \sinh K,\quad 0 \le \phi' \le \pi,\quad 0 \le \theta' \le 2\pi \tag{3-2}$$

and a weighting factor:

$$w = K^d \tag{3-3}$$

for each set, where K is the Fisher dispersion parameter for the set. The probability of an orientation being assigned to a particular set i is given by:

$$P[i|\phi,\theta] = k_i \,/\, \sum_i k_i \tag{3-4}$$

where k_i is the weighting factor times the value of the p.d.f.

After assigning the fractures to sets, the mean direction and Fisher dispersion parameter are recalculated for each set, and displayed on the screen. ISIS also calculates the Kolmogorov-Smirnov (K-S) test statistic for the fitted distribution, and ISIS uses the new set of Fisher distribution parameters to reassign the fractures. This process of regrouping the fractures is repeated until the distribution parameters of the sets stabilize.

A preliminary stereonet plot of the Terzaghi-corrected pole data (Figure 3-1) indicated the presence of three well-defined sets with mean pole directions of roughly (290,10), (225,10), and (90,90), plus a fourth, poorly-defined set to account for the remaining fractures. ISIS was used to identify these sets automatically, by assigning initial pole directions of (90,90) and Fisher dispersions of 1.0 to all four sets, and then allowing ISIS to iteratively reassign fractures to sets until four distinct, stable sets were found. After more than 200 iterations, ISIS converged to the set of values given in Table 3-1. The sets identified by ISIS corresponded approximately to the sets identified by Gale (1989). The correspondence is indicated in Table 3-1. Of the sets identified by ISIS, Sets 1, 2, and 4 correspond approximately to the sets at (225,10), (290,10), and (90,90), respectively, that were identified by inspection of the plot in Figure 3-1.

Table 3-1. Distribution Parameters for Four Fracture Sets Identified from the Full Orientation Data Set (automatic set identification by ISIS).

Set	Gale Set	Mean Pole Direction (azimuth, inclination)	Fisher Dispersion Parameter K	Kolmogorov-Smirnov Statistic	Significance Level for K-S Statistic
1	A	222.6, 15.6	5.46	0.047	0.096
2	B	271.1, 22.9	7.96	0.037	0.124
3	C1	116.6, 12.1	7.29	0.034	0.309
4	C2	279.1, 80.9	7.17	0.096	4.0e-8

The Fisher distribution was used in classifying the fractures into sets because of the simplicity of its form, which allows simple estimation of the distribution parameters (Cheeney, 1983). The Fisher distribution is applicable to directional data because it is defined on a sphere. A distribution defined on a plane, such as a bivariate normal distribution for strike and dip, is inappropriate for directional data because a mapping of spherical data onto a plane produces distortions in the density of data points.

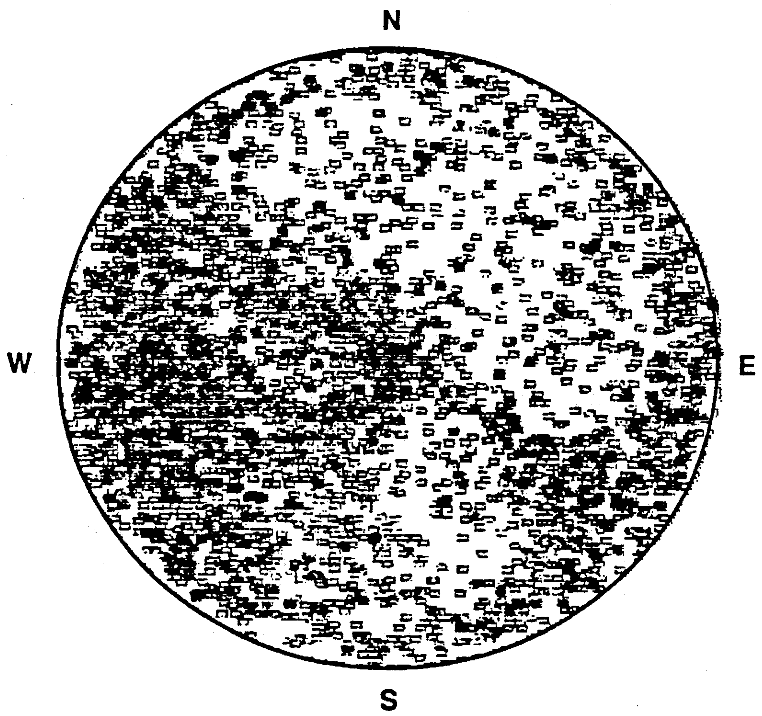

FIGURE 3-1
FRACTURE POLES FROM SCANLINES 1-7 AND BOREHOLES N1, N2, N3, N4, W1, AND W2, AFTER APPLYING TERZHAGI CORRECTION
STRIPA

With the exception of Set 4, the set assignments in Table 3-1 are acceptable at a significance level of five percent or higher. The high values of the Kolmogorov-Smirnov test statistics for Set 4, the most concentrated set, indicate that a Fisher distribution does not give a very good fit to the data for this set. This set consists mainly of subhorizontal fractures that were only sparsely sampled by the characterization program (Gale and Stråhle, 1988), since these fractures were roughly parallel to the boreholes and scanlines. While the modified Terzaghi correction used was intended to compensate for sampling bias due to orientation, the correction cannot entirely compensate for extreme sampling biases due to "blind zones" such as those indicated for these data by Gale and Stråhle (1988). For this reason, and because better fits for Set 4 were not obtained by varying the value of d, the distribution parameters for Set 4 found by ISIS were accepted in spite of the relatively poor K-S statistics.

3.3 CONDUCTIVE FRACTURE FREQUENCY AND TRANSMISSIVITY

The transmissivity distribution and frequency of the conductive fractures along the N- and W- holes was determined from fixed-interval-length (FIL) tests, by using an approach adapted from Osnes et al. (1988). The method assumes that the net transmissivity of a test zone is equal to the sum of the transmissivities of the conductive fractures that intersect the test zone (Figure 3-2):

$$T_i = \sum_{j=1}^{n_i} T'_{ij} \tag{3-5}$$

where

T_i = the measured transmissivity of the ith test zone
T'_{ij} = the apparent transmissivity of jth fracture in the ith test zone, (the transmissivity "seen" by the borehole)
n_i = the number of conductive fractures intersecting the ith test zone

The location of conductive fractures along the borehole is assumed to be a stationary, Poisson process, so that the number of conductive fractures n_i within a given test zone is a random number defined by a Poisson distribution (Benjamin and Cornell, 1970):

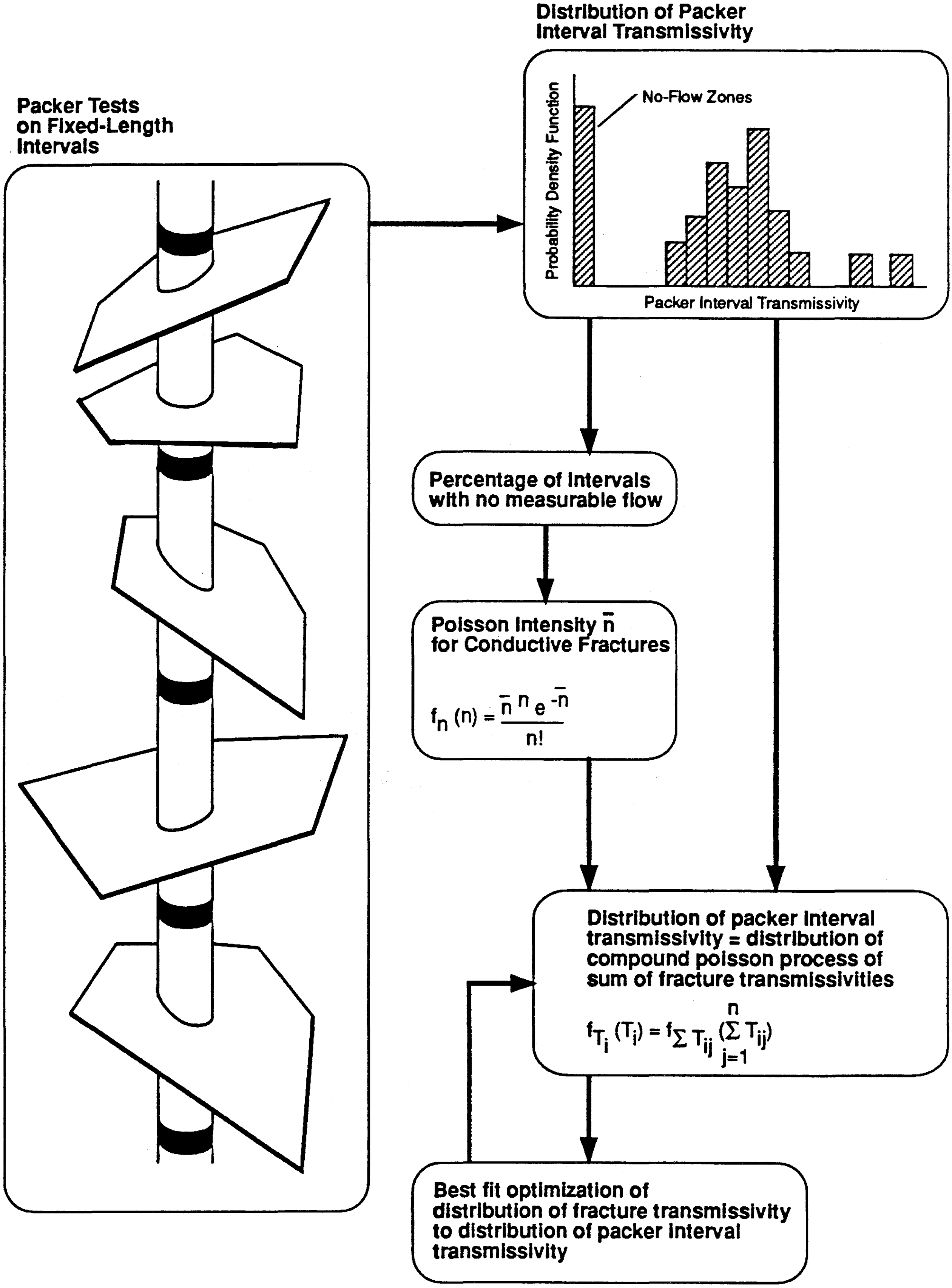

FIGURE **3-2**

FIXED-INTERVAL-LENGTH PACKER TEST INTERPRETATION APPROACH

STRIPA

PROJECT NO. 883-1313.220 DWG. NO. 00000 DATE 4/10/90 DRAWN CB

Golder Associates

$$f_n\ (n_i) = \frac{\bar{n}^{n_i}\ e^{-\bar{n}}}{n_i!} \qquad (3\text{-}6)$$

where

$\bar{n}$ = the mean number of conductive fractures within a test zone (i.e., the expected value of n_i).

The transmissivities of individual fractures are assumed to be randomly distributed according to a particular distributional form $f_T\ (T_{ij})$. The distribution of single-fracture transmissivities T_{ij} is assumed to be independent of location along the boreholes. In the present study, a lognormal distributional form was used for T'_{ij}, i.e., it was assumed that log T_{ij} is normally distributed, with mean $\mu_{\log T}$ and standard deviation $\sigma_{\log T}$. The lognormal distributional form was selected based upon the Pearson statistics for the distribution of test-zone transmissivities T_i.

In this approach, the transmissivity of the ith test zone T_i is taken to be the sum of a random number of random values. Therefore the distribution of T_i is a compound Poisson process (Feller, 1971). For the case of lognormally distributed T'_{ij}, T_i is the sum of a random number of lognormal variate. The parameters $\bar{n}$, $\mu_{\log T}$, and $\sigma_{\log T}$ are estimated by iterative simulation, as depicted in Figure 3-3. The final estimates of these statistics are given in Table 3-2.

Table 3-2. Conductive Fracture Frequency and Transmissivity Statistics from Forward Modeling Using @RISK

	Log_{10} Mean (m^2/s)	Log_{10} Std Dev (m^2/s)	Frequency (m^{-1})	ChiSquared Statistic (-)	Significance Level
N-holes	-10.5	1.5	0.57	25.17	0.087
W-holes	-9.5	1.5	0.57	22.29	0.215

One important deficiency in the analysis performed for the SDE simulations was that the analysis did not account for local variability of fracture transmissivity due to variations in fracture aperture or infilling. The transmissivity of a fracture as observed in a borehole test T'_{ij} is not necessarily equal to T_{ij}, the average transmissivity of the fracture (Kenrick et al., 1989). Numerical simulations performed by Kenrick et al. demonstrated that the observed

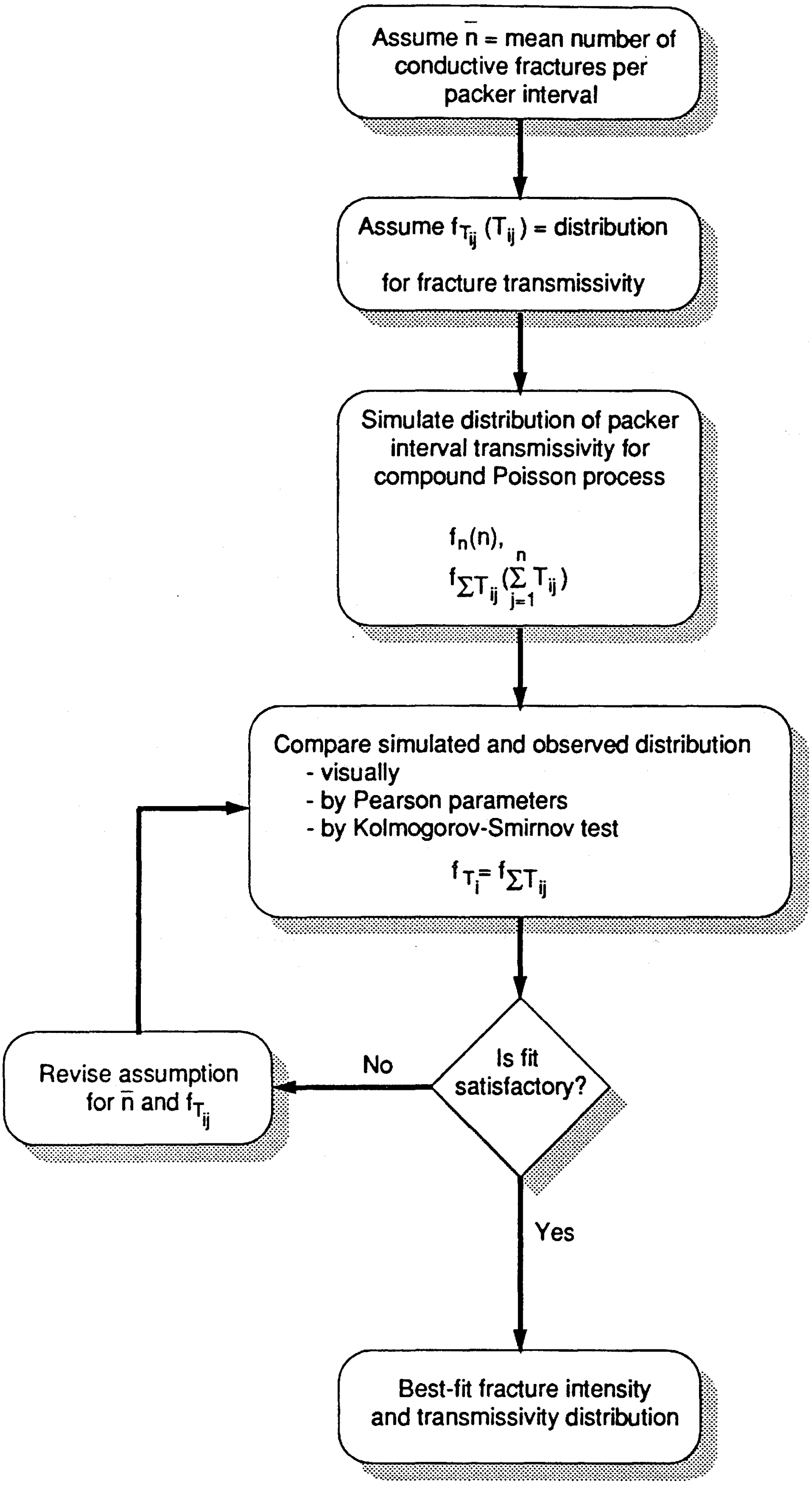

FIGURE **3-3**

MONTE CARLO SOLUTION FOR FRACTURE TRANSMISSIVITY AND INTENSITY

STRIPA

PROJECT NO. 883-1313.220 DWG. NO. 00000 DATE 4/10/90 DRAWN CB

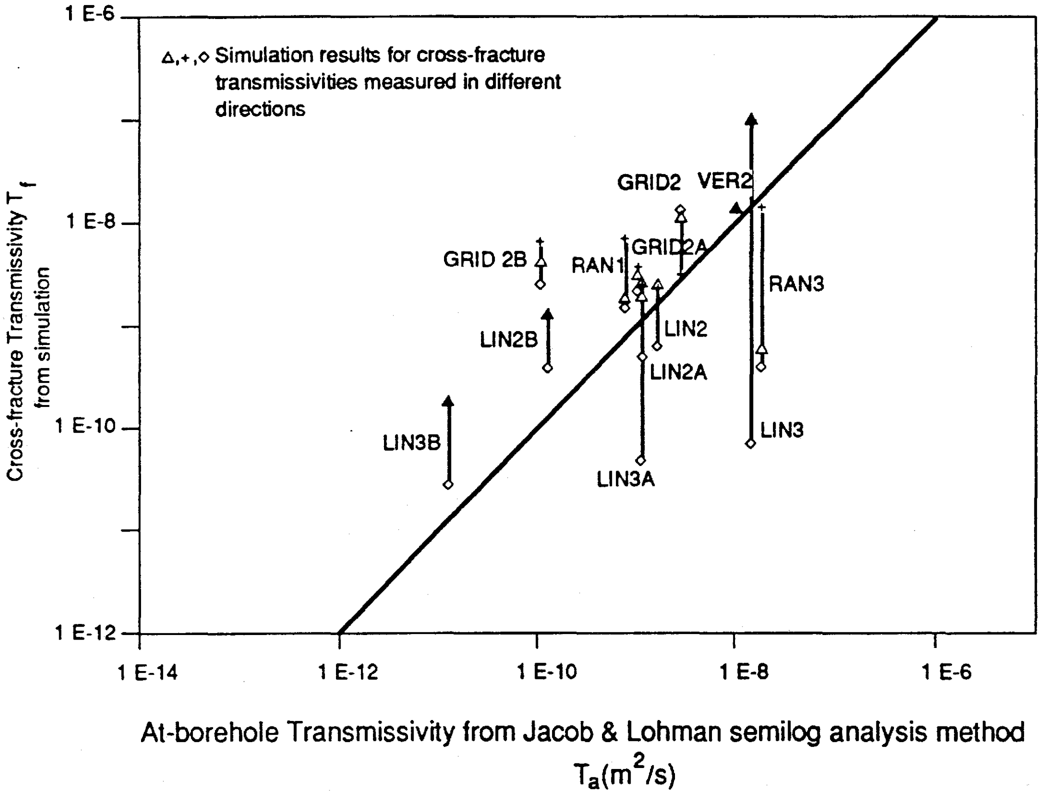

LIN, GRID, VER, and RAN indicate different structures of local variability in fracture aperture as described in Kenrick et al. (1989).

FIGURE **3-4**

AVERAGE FRACTURE TRANSMISSIVITY (Tf) VERSUS TRANSMISSIVITY FROM ANALYSIS (Ta)

STRIPA

PROJECT NO. 883-1313.220 DWG. NO. 22064 DATE 4/10/90 DRAWN CB

T'_{ij} may be much less than the average T_{ij} if the borehole intersects the fracture at a point with low local conductivities. Conversely, if the borehole intersects the fracture at a point with relatively high transmissivities, the observed T'_{ij} may be considerably higher than the average T_{ij}. Figure 3-4 (adapted from Kenrick et al., 1989) shows the ranges in values of "average" transmissivites (T_f in the figure) that were measured by simulating flow from one side of a hexagonal fracture to the opposite side, for different fracture orientations and for several different patterns of transmissivity variation. The average transmissivities are plotted versus the "observed" transmissivities calculated by type-curve analyses (T_a in the figure).

The effect of variations in local transmissivity can be incorporated in this methodology for deriving the parameters of the fracture transmissivity distribution, by explicitly accounting for the uncertainty in the probabilistic relationship between T_{ij} and T'_{ij}. The form and parameters of this relationship can be estimated from numerical results such as those shown in Figure 3-4. These parameters can then be used in a Monte Carlo approach to simulate the distribution of T'_{ij} from an assumed distribution of T_{ij}. In the analysis that was performed for this SDE prediction, the distributions of T_{ij} and T'_{ij} were assumed to be identical, but this will be corrected in the analysis of data for the SCV Drift inflow prediction.

3.4 STORATIVITY

The storativity of fractures is needed to predict the transient response of the fracture network during the simulated drift experiment. Although a precise knowledge of fracture storativity is not critical to the steady-state inflow predictions that are the main goals of this modeling exercise, a rough estimate of storativity is needed to estimate the time needed to achieve steady-state conditions in this experiment.

Accurate values for storativity of fractures are difficult to determine from inversion of hydrological testing data, due to wellbore storage effects and uncertainty about flow geometries. A rough estimate of single-fracture storativity can be obtained by dividing the apparent storativities of packer test intervals by the conductive fracture frequency f_c. Table 3-3 gives storativities estimated from crosshole tests between the N4 borehole and the W1 borehole (data from Patrick, 1989), assuming a conductive fracture frequency of 0.57 fractures per meter. The mean single-fracture storativity estimated from these data is 1.0×10^{-8} (dimensionless). The use of a single, average value for fracture storativity in transient tests ignores variability and correlations with transmissivity that will exist in a real fracture population. Thus any prediction of the transient response made using these data should be seen only as a rough estimate.

Table 3-3. Preliminary storativity estimates from crosshole hydrological testing

N4 Interval	W1 Interval	Interval Storativity (-)	Estimated Single Fracture Storativity (-)
77 - 108m	92 - 105m	2.77×10^{-7}	1.56×10^{-8}
77 - 108m	76 - 91m	1.85×10^{-7}	1.04×10^{-8}
77 - 108m	55 - 75m	0.94×10^{-7}	0.53×10^{-8}

3.5 SIZE AND SHAPE

In this exercise, fractures were assumed to be polygonal approximations for disk-shaped features, without terminations at intersections with other fractures. In the FracMan package, circular fractures are represented approximately by regular hexagons of areas equal to the areas of the circles. The assumption of circular, non-terminating fractures was adopted because the available data were not sufficient for quantifying fracture shape in terms of ellipticity or termination statistics. The probability distributions for fracture radius were inferred from trace-length data, making a series of corrections for censoring, truncation, and sampling bias.

Preliminary analysis of trace length data was performed by Gale (1989), who divided the fractures into four sets A, B, C1, and C2 corresponding approximately to the ISIS-derived Sets 1, 2, 3, and 4, respectively. Assuming a log normal distribution of trace lengths, Gale corrected the original scanline data for the effects of censoring and truncation. The parameters of the resulting log normal distributions for trace length are given in Table 3-4.

Table 3-4. Log normal distribution parameters for trace length, corrected for censoring and truncation effects by Gale (1989).

Set	Trace length	
	Log Mean $\mu_{\ln L}$ (m)	Log Std. Dev. $\sigma_{\ln L}$ (m)
A	-0.36	1.47
B	-1.53	0.98
C1	-1.95	1.38
C2	-0.63	1.72

The parameters of lognormal distributions for radius corresponding to the trace length distributions were determined by forward modeling using @RISK, as depicted in Figure 3-5. This method simulates the relation of trace length to fracture radius, and incorporates the effects of sampling bias due to fracture size. The input to this model consists of the log mean $\mu_{\ln r}$ and log standard deviation $\sigma_{\ln r}$ for radius, and the number of iterations for the simulation. The model generates random values for radius, fracture dip angle, and distance from a plane, and calculates the lengths of intersections between the simulated fractures and the plane. The input parameters are varied manually until an acceptable match to the trace length distribution is obtained.

The spreadsheet uses a simplified model of fracture geometry to simulate fracture trace lengths, as illustrated in Figure 3-6. The radius R is assumed to be lognormally distributed:

$$r \sim LN\ (\mu_{\ln r}, \sigma_{\ln r}) \qquad (3\text{-}7)$$

The distance x between the center of the fracture and the traceplane is uniformly distributed:

$$x \sim U\ (0, r_{max}) \qquad (3\text{-}8)$$

The angle α between the normal to the fracture and the normal to the traceplane (Figure 3-6) is taken to be uniformly distributed:

$$\alpha \sim U\ (\pi/2 - \phi, \pi/2),$$

where

ϕ = the mean dip angle for the set.

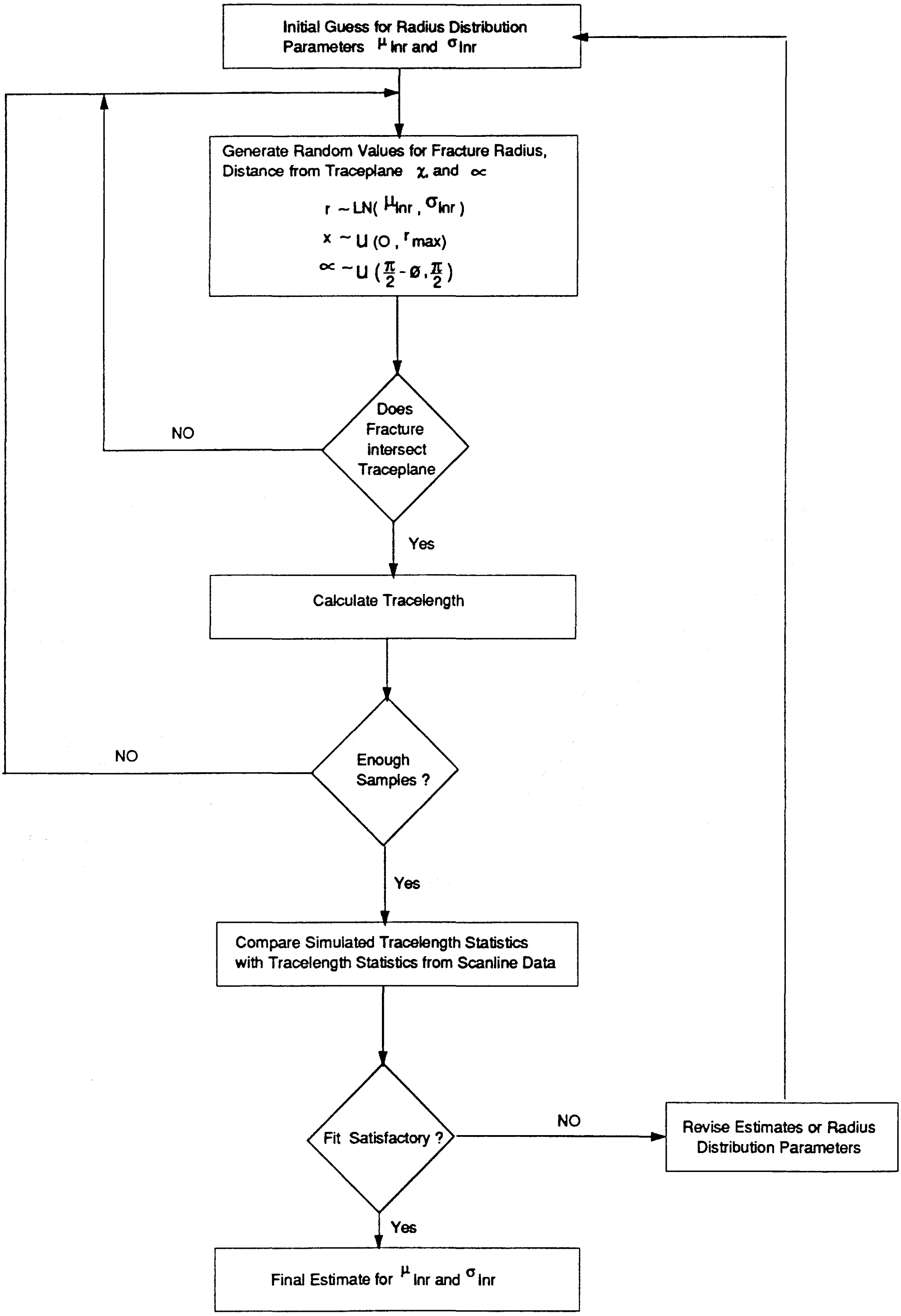

FIGURE **3-5**

METHOD OF DETERMINING FRACTURE RADIUS STATISTICS BY FORWARD MODELING TO MATCH TRACELENGTH STATISTICS

STRIPA

ROJECT NO. 883-1313.220 DWG. NO. 00000 DATE 4/25/90 DRAWN DC

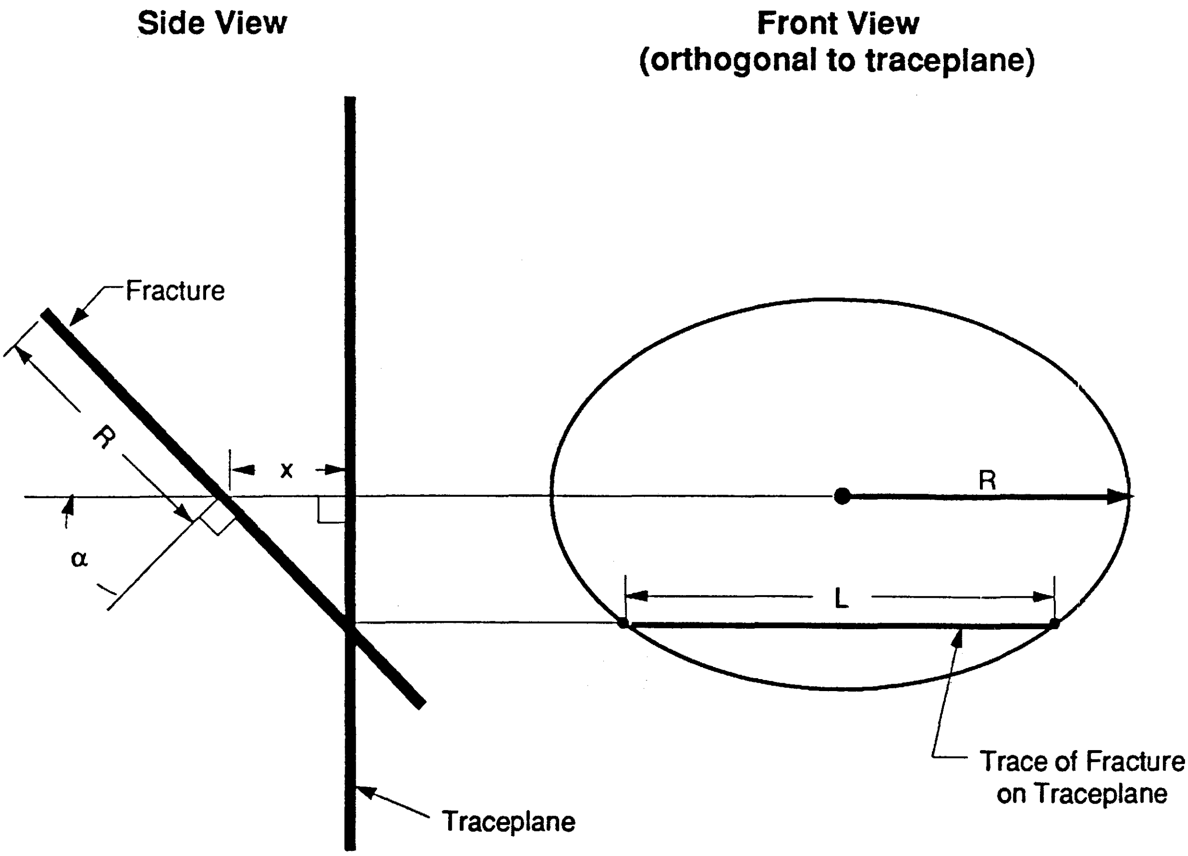

FIGURE **3-6**
INTERSECTION BETWEEN A CIRCULAR FRACTURE AND AN INFINITE TRACEPLANE
STRIPA

The use of a uniform distribution for α is only a crude approximation to the actual distribution of α, which would depend upon the Fisher distribution parameters for pole direction, as well as the orientations of traceplanes and the relative lengths of scanlines of different orientations. The use of a uniform distribution ranging between perpendicular to the traceplane and parallel to the mean dip angle is somewhat artificial, but is justified in part by the fact that fractures at angles outside of this range are poorly sampled in the scanline data.

An intersection between a simulated fracture and the traceplane occurs if:

$$x < r \cos (\pi/2 - \alpha) \tag{3-9}$$

in which case the tracelength is given by:

$$L = [r^2 - x^2 / \cos^2 (\pi/2 - \alpha)]^{1/2} \tag{3-10}$$

Table 3-5 gives the parameters of the radius distributions for each of the four sets. The uncertainty in the estimates of these parameters is quite high due to the crudeness of the method for simulating tracelength statistics.

Table 3-5. Lognormal distribution parameters for fracture radius, determined by forward modeling using @RISK spreadsheet.

Set	Fracture Radius Log Mean $\mu_{\ln r}$ (m)	Fracture Radius Log Standard Deviation $\sigma_{\ln r}$ (m)
A	-1.07	1.14
B	-1.34	1.05
C1	-0.64	1.02
C2	-1.51	1.23

These values were used as the parameters of truncated lognormal distributions for fracture radii. Fracture radii were simulated from the lognormal distributions defined by the parameters in Table 3-5, and radii outside of the interval:

$$r_{min} < r < r_{max}$$

were discarded. Since all fracture properties were considered to be independent of each other in these simulations, this procedure was equivalent to generating fractures with lognormally-varying radii, and then discarding all fractures having radii outside of this interval.

A maximal fracture radius r_{max} = 50 m was assumed for both the inner and outer subregions. This was assumed to be roughly the scale of the largest fracture that would have escaped detection as a major feature during site characterization. A fracture of radius larger than 50 m would have a diameter within one order of magnitude of the scale of the granite intrusion in the vicinity of the mine. In terms of trace-length statistics, truncating these radii distributions above 50 m does not produce any significant effect on the match to trace-length statistics, since in these distributions less than one fracture in 10,000 would exceed this size, and since severe truncation of trace lengths would occur in mapping these fractures on 3m-high trace planes.

A lower bound on the fracture size distribution was necessary in order to avoid generating a multitude of very small fractures that would exceed the capacity of the computers used in this exercise. For the inner region, a minimal radius r_{min} = 1 m was selected. Fractures of radius less than this would account for only a small fraction of the total fracture area resulting from the untruncated lognormal distributions of radii. For lognormal distributions with parameters as specified for Sets A, C1, and C2, fractures of radius less than 1 m would account for less than five percent of the total fracture area; for Set B these fractures would account for less than ten percent of the total area. Despite the relatively small fraction of the total intensity represented by these smaller fractures, they may still be hydrologically significant since they may occasionally provide the critical connections between larger fractures. However, this effect is probably small relative to the possible effects of errors in estimates of the parameters of the size distributions.

For the outer region, a minimal radius r_{min} = 5 m was used. This represents a more significant departure from the radius distributions that were derived from tracelength statistics. Fractures of radius less than 5 meters account for approximately 10 percent of the total fracture area resulting from the derived distributions for Sets A, C1 and C2, and approximately 25 percent of the total area for Set B. The effects of this were compensated for by calibrating the model against observed fluxes into boreholes and drifts, as is described in Section 4.2.

3.6 CONDUCTIVE FRACTURE INTENSITY

The density of fractures within the region of the model can be described in terms of the areal fracture intensity. As defined by Dershowitz (1984), the areal intensity is the total area of fractures per unit volume of rock:

$$P_{32} = \sum_{i=1}^{N} A_i/V \tag{3-11}$$

where

A_i = the area of the ith fracture

N = the number of fractures in the region

V = the volume of the region.

The conductive fracture intensity P_{32c} is the fraction of P_{32} given by:

$$P_{32c} = \sum_{j=1}^{N_c} A_j/V \tag{3-12}$$

where

A_j = the area of the jth conductive fracture

N_c = the number of conductive fractures in the region.

The intensity measure P_{32} was selected because it is invariant. The P_{32} for each set was calculated from the mean fracture frequency (the number of fractures per meter of borehole length), f, observed in the N- and W-holes. The relationship between of f and P_{32} depends upon the orientation distribution of fractures relative to the borehole. For fractures with a uniform distribution of orientation, the relationship is (Dershowitz, 1984)

$$P_{32} = 2f. \tag{3-13}$$

Where the distribution of orientation for a fracture set is known the relationship between f and P_{32} can best be found by simulation, using the FracMan simulated borehole sampling feature to explicitly account for the effects of directional bias.

Fractures were simulated according to the orientation and fracture-size statistics described in Sections 3.2 and 3.5. A set of four simulated boreholes was used to sample these fractures to determine the relationships between fracture frequency and fracture intensity. One of the boreholes was parallel to the direction of the N-holes. The other three were parallel to the directions of the W-holes. The total lengths of the two sets of boreholes were scaled down (to reduce the number of fractures needed in the simulation), such that the ratio of W-hole total length to N-hole total length was preserved. The collar coordinates, lengths, and directions of the simulated boreholes are given in Table 3-6.

Table 3-6. Simulated boreholes used to determine relationship between fracture frequency and fracture intensity.

Collar Coordinates x	y	z	Direction	Length (m)
0	15	2	270, 0	29.4
10	-10	6.3	0, 18	20.5
10	0	6.3	0, 18	20.5
10	10	6.3	0, 18	20.5

It was assumed that for each set the statistical relationship between fracture frequency and fracture intensity is of the form:

$$f = g(\theta, \phi, K, \mu_{lnr}, \sigma_{lnr}) P_{32}, \qquad (3\text{-}14)$$

where:

θ, ϕ = the mean pole direction of the set,

K = the Fisher dispersion, and

μ_{lnr}, σ_{lnr} = parameters of the fracture size distribution,

and where $g(\theta, \phi, K, \mu_{lnr}, \sigma_{lnr})$ is independent of P_{32}. Seven simulations were performed for each fracture set. The results of these simulations are summarized in Table 3-7.

The conductive fracture intensity P_{32c} for each set was estimated by assuming the percentage of fractures that are conductive is the same in each set. Since the conductive fracture frequency measured in the N- and W-holes was 4.0 fractures per 7 meter interval (= 0.57 m^{-1}) and the total fracture frequency determined from core logs was $f = 4.18\ m^{-1}$ (from Gale, 1989):

$$P_{32c} = (f_c / f)\, P_{32} = (0.57 / 4.18)\, P_{32} = 0.137\, P_{32} \qquad (3\text{-}15)$$

Table 3-7. Estimates of conductive fracture intensity from observed fracture frequencies along boreholes.

Set	Observed f^* (m^{-1})	f/P_{32}	Estimated P_{32} (m^2/m^3)	Estimated P_{32c} (m^2/m^3)
A	0.49	0.54	0.89	0.12
B	2.86	0.47	6.06	0.83
C1	0.40	0.36	1.11	0.15
C2	0.44	0.53	0.82	0.11
Total	4.18	--	8.49	1.21

* - Observed f = [observed spacing from Gale, 1989 $]^{-1}$

3.7 TERMINATION

The fractures used in the present model are polygonal approximations to circular, disk-shaped fractures, with no terminations of fractures at intersections. This introduces an error into the model, because a high percentage of the fractures at the SCV site are observed to terminate at intersections with other fractures. Gale (1988) reports that 70% to 90% of the fractures in each set that were mapped along scanlines terminate against other fractures.

The omission of fracture termination effects from the model most probably has the effect of diminishing the connectivity of the modeled system. When fracture populations are simulated to match trace-length statistics, a model that does not include terminations at intersections will produce connectivities that are systematically lower than the connectivities of the real fracture populations (Geier et al., 1988). For the purposes of producing this influx prediction, the effect of this simplification will be to reduce the predicted influxes, and to reduce the number of points along the D-holes at which inflow occurs. The magnitude of this effect cannot be assessed without a comparison of runs with and without termination effects.

Termination effects were omitted from the model for this inflow prediction, due to the additional time that would be required to develop the appropriate termination statistics and to generate fractures with terminations at intersections according to the Enhanced Baecher model. The termination statistics developed by Gale (1988) are not directly applicable to the Enhanced Baecher model because they are stated in terms of the percentages of fractures that terminate at an intersection with some other fracture, whereas the Enhanced Baecher model requires the probability that a fracture terminates at any given intersection with a fracture of another set. The termination probabilities required for the Enhanced Baecher model can be estimated from the termination percentages observed on traceplanes. These estimates of termination probabilities must be refined by forward modeling using simulated traceplane sampling to account for the differences between the true termination probability in three dimensions and the observed termination percentages in a two-dimensional traceplane. Termination statistics will be derived for the detailed SCV prediction, which will utilize the Enhanced Baecher model.

The compilation of termination statistics for the Enhanced Baecher model involves the following steps:

- classification of fractures by set on trace maps

- counting of intersections and terminations of fractures at intersections

- forward modeling using simulated traceplane sampling to determine the actual fracture termination and size distribution statistics, using as initial estimates the terminated percentages on traceplanes and the fracture size distribution statistics that were derived using the assumption of no terminations at intersections.

The process of forward modeling to derive termination statistics, and the subsequent generation of fracture populations for hydrological modeling are computationally intensive tasks, because of the additional calculations needed to determine fracture intersections when generating fractures according to the Enhanced Baecher model.

3.8 LOCATION

The site characterization program identified six major fracture zones, as depicted in Figure 1-3. These fracture zones were included in these simulations by locating fractures according to the FracMan deterministic War Zone model, which produces a non-uniformly random distribution of fracture locations in 3-D space. In the deterministic War Zone model, tabular zones of elevated fracture intensity are created with orientations and thicknesses to match observed fracture zones. Within these zones fractures are uniformly, randomly located with areal intensity P_{32cw}. Outside of these zones fractures are uniformly, randomly located with areal intensity:

$$P_{32co} = (P_{32c}V - P_{32cw}V_w) / (V - V_w) \qquad (3\text{-}16)$$

where

V = total volume of the modeling region

V_w = volume of the "war zones"

This model gives an average fracture intensity of P_{32c}.

For these simulations, the ratio P_{32cw}/P_{32co} was estimated from fracture spacing data along the N- and W-holes, by comparing fracture frequencies within the zones with fracture spacings outside of the fracture zones:

$$P_{32cw}/P_{32co} = f_w/f_o = f_w (L - L_w) / (fL - f_wL_w) \qquad (3\text{-}17)$$

where:

L = total length of the boreholes

L_w = total length of boreholes in fracture zones

f_o = the average fracture frequency outside of the fracture zones.

f_w = the average fracture frequency in the fracture zones.

The quantities f_w and L_w were determined from corelog data by counting the number of fractures in the intervals within the fracture zones, using the data given by Olsson et al., 1989 (Table 3-8) to determine the intervals within fracture zones along the boreholes.

All of the fracture zones were treated alike despite indications to the contrary, both from core logs and from hydrological tests in the N- and W-holes. Table 3-9 gives the relative fracture frequencies determined from core logs for each zone, expressed as the ratios of fracture frequency inside the zones to the fracture frequency outside of all fracture zones. The relative fracture frequencies at the sampled locations in Zones GA are somewhat higher than for the other zones, while for Zones GB and GC the relative frequencies are anomalously low. Olsson et al. (1989) found that Zones GB, GC, GHa, GHb, and GI have anomalously high mean transmissivities, while Zone GA has a lower mean transmissivity.

Table 3-8. Intersections of major features with N- and W-holes.

Borehole	Feature	Intersection
N2	GB	184 - 190m
N3	GC	45 - 48m
	GB	130 - 135m
	GA	163 - 171m
N4	GC	23 - 29m
	GB	123 - 129m
	GA	153 - 156m
W1	GHa	45 - 53m
	GHb	58 - 64m
	GI	108 - 112m
	GB	132 - 137m
W2	GHa	50 - 57m
	GHb	67 - 72m
	GB	87 - 92m
	GI	127 - 130m
	GA	140 - 145m

Table 3-9. Relative fracture frequencies in major features

Borehole	Feature	f_w/f_o (-)
N2	GB	0.46
N3	GC	0.00
	GB	1.26
	GA	1.17
N4	GC	0.55
	GB	1.22
	GA	1.60
W1	GHa	2.06
	GHb	2.23
	GI	1.64
	GB	1.52
W2	GHa	1.91
	GHb	1.67
	GB	1.52
	GI	2.36
	GA	4.20
Averages	GA	2.21
	GB	1.37
	GC	0.36
	GHa	1.99
	GHb	1.98
	GI	1.95

The differences in observed fracture frequencies and transmissivities among the identified fracture zones may or may not be indicative of pervasive differences in properties between zones. While measurements taken from the few points at which the zones are intersected by boreholes would indicate that some of the zones are more conductive than others, it is possible that the differences merely reflect heterogeneities within the fracture zones. Even if within a given fracture zone the fracture properties were statistically uniform, regions of relatively high or low transmissivity would be expected within the zone. For this reason, and in order to simplify the analysis, all fracture zones were treated equally in the present study.

If the characteristics of the identified fracture zones are in fact significantly different, this would affect the spatial distribution of flux along the D-holes, since this circumstance would result in more inflow from the more well connected, transmissive fracture zones.

The anomalously low transmissivities in Zone GA, the zone which had the highest fracture frequencies in core logs, raises some question about the method used here to determine the conductive fracture frequencies for the fracture zones. The method is based upon observed fracture frequencies and not on conductive fracture frequencies. A more appropriate method may be to employ the maximum likelihood approach described in Section 3.3 to determine the conductive fracture frequencies for the zones, by considering the FIL test intervals within the fracture zones separately from the remaining zones. This approach was not used in the present modeling effort, but will be employed in predicting the flux into the Validation Drift in the later stages of the Phase 3 project.

4 STOCHASTIC SIMULATIONS

4.1 SIMULATION DEFINITIONS

Two stages of Monte Carlo simulations were needed to predict the flux into the D-holes. Preliminary simulations were needed to check the transmissivity distributions for the outer, sparse fracture network, and to calibrate the parameters of the distributions. After calibrating these parameters, the flux predictions were obtained by producing multiple, random realizations of the fracture populations using FracMan, and solving the flow equations for each realization using MAFIC.

Calibration to determine the parameters for the outer region was performed by comparing inflows predicted by the model with inflows measured in the 3-D Migration Experiment Site (Drifts 10 and 11 in the model) by Abelin et al. (1989) and in the N2, N3, N4, W1 and W2 holes by Wikberg et al. (1985). In the calibration runs the distributions and parameters that defined the fracture population were initially as derived in Chapter 3, with values as summarized in Table 4-1. The transmissivity distribution was adjusted by scaling the transmissivity of fractures in the outer region by a factor m_T, in order to determine the best value of m_T by a trial-and-error process.

Three suites of calibration runs were carried out, using factors of 1, 5, and 10. A comparison of the measured inflows with the inflows predicted by the calibration runs is given in Table 4-2. The fluxes into the W2 borehole as predicted by the calibration runs borehole were not used in the calibration, because of the proximity of the W2 hole to the outer boundary of the model. However, the flux measured into this hole by Wikberg et al. (1988) is given in the table for the sake of comparison.

Table 4-1. Dataset for inner and outer subregions

	Set A	Set B	Set C1	Set C2
Inner Subregion:				
Orientation distribution	Fisher	Fisher	Fisher	Fisher
Mean pole azimuth	222.6	271.9	279.1	116.6
Mean pole inclination	15.6	22.9	80.9	12.1
Dispersion parameter	5.46	7.96	7.17	7.29
Fracture radius	Truncated LogNormal	Truncated LogNormal	Truncated LogNormal	Truncated LogNormal
Mean Radius (m)	0.66	0.45	0.89	0.47
Standard Deviation (m)	1.07	0.64	1.20	0.89
Minimum Radius (m)	1.0	1.0	1.0	1.0
Maximum Radius (m)	50.0	50.0	50.0	50.0
War zone intensity	1.6	1.6	1.6	1.6
Termination percentage	0	0	0	0
Intensity (m^{-1})	0.54	0.329	0.069	0.049
Fracture Transmissivity	Truncated LogNormal	Truncated LogNormal	Truncated LogNormal	Truncated LogNormal
Mean (m^2/s)	1.23×10^{-7}	1.23×10^{-8}	1.23×10^{-8}	1.23×10^{-8}
Standard deviation (m^2/s)	4.8×10^{-5}	4.8×10^{-6}	4.8×10^{-6}	4.8×10^{-6}
Minimum Transmissivity (m^2/s)	3.2×10^{-10}	3.2×10^{-11}	3.2×10^{-11}	3.2×10^{-11}
Maximum Transmissivity (m^2/s)	1.0	1.0	1.0	1.0
Storativity	1×10^{-8}	1×10^{-8}	1×10^{-8}	1×10^{-8}

Table 4-1. Dataset for inner and outer subregions (Continued)

	Set A	Set B	Set C1	Set C2
<u>Outer Subregion</u>:				
Orientation distribution	Fisher	Fisher	Fisher	Fisher
Mean pole azimuth	222.6	271.9	279.1	116.6
Mean pole inclination	15.6	22.9	80.9	12.1
Dispersion parameter	5.46	7.96	7.17	7.29
Fracture radius	Truncated Lognormal	Truncated Lognormal	Truncated Lognormal	Truncated Lognormal
Mean Radius (m)	0.66	0.45	0.89	0.47
Standard Deviation (m)	1.07	0.64	1.20	0.89
Minimum Radius (m)	7.5	7.5	7.5	7.5
Maximum Radius (m)	50	50	50	50
War zone intensity	1.6	1.6	1.6	1.6
Termination percentage	0	0	0	0
Intensity (m^{-1})	0.122	0.829	0.152	0.113
Fracture Transmissivity	Truncated LogNormal	Truncated LogNormal	Truncated LogNormal	Truncated LogNormal
Mean (m^2/s)	$1.23x10^{-7}$	$1.23x10^{-8}$	$1.23x10^{-8}$	$1.23x10^{-8}$
Standard deviation (m^2/s)	$4.8x10^{-5}$	$4.8x10^{-6}$	$4.8x10^{-6}$	$4.8x10^{-6}$
Minimum Transmissivity (m^2/s)	$1.0x10^{-10}$	$1.0x10^{-11}$	$1.0x10^{-11}$	$1.0x10^{-11}$
Maximum Transmissivity (m^2/s)	1.0	1.0	1.0	1.0
Storativity	1×10^{-8}	1×10^{-8}	1×10^{-8}	1×10^{-8}

Table 4-2. Comparison of Measured and Predicted Inflows from Calibration Runs

Measurement Point	Measured Inflow (l/hr)	Inflow Predicted by Calibration Runs (l/hr)		
		$m_T = 1$	$m_T = 5$	$m_T = 10$
N2 Borehole	9.4	< 0.1	0.4	56.1
N3 Borehole	10.0	0.5	< 0.1	9.0
N4 Borehole	22.8	< 0.1	9.2	19.4
W1 Borehole	15.2	< 0.1	44.7	268.3
W2 Borehole	149.7	--	--	--
3-D Drift	3.1	6.6	9.4	29.4
Euclidean distance	-	30.7	35.6	258.7
Logarithmic distance	-	4.0	2.2	1.8

The correctness of the calibration was assessed in terms of two measures: the Euclidean "distance" and the logarithmic "distance" between the vectors of predicted and measured fluxes for all measurements points, where the Euclidean distance is defined as:

$$\sqrt{\left[\sum_i (Q_{mi} - Q_{pi})^2\right]}$$

and the logarithmic distance is defined as:

$$\sqrt{\left[\sum_i (\log Q_{mi} - \log Q_{pi})^2\right]}$$

where

Q_{mi} = measured value of flux for the *i*th measurement point

Q_{pi} = predicted value of flux for the *i*th measurement point

In the first calibration suite,the original distribution of transmissivities for the outer region was used, so that the effective value of m_T was unity. This produced fluxes that were only about 12 percent of the measured fluxes, on average. Hence it was decided that a factor of unity was too low. In the second calibration suite, the factor m_T was increased to ten; this produced fluxes that were generally higher than the observed fluxes, which suggested that the best value of m_T lay between 1 and 10. In the third suite, m_T was reduced to 5, which gave fluxes that were reasonably close to the data of Abelin et al. (1989) and Wikberg et al. (1988), both in terms of the Euclidean distance and the logarithmic distance between measured and observed fluxes. Inspection of the values in Table 4-2 suggests that the best value of m_T probably lies between 5 and 10. This could be tested by additional simulations for intermediate simulations. However, due to a limit on the time available for calibration, the factor $m_T = 5$ was used in the final simulation runs.

4.2 ANALYSIS

26 Monte Carlo simulations were performed for this flow prediction exercise. The form of the output from these simulations was a list of fluxes at nodes along the D-holes. Figure 4-1 shows a histogram of the fluxes for 1-meter intervals along each of the outer D-holes, obtained from a single simulation. The flux to the D1 borehole is not shown; in the simulations this flux was generally less than 0.005 liters per hour, which is on the order of the numerical errors in the model. The locations of the predicted intersections of the D-holes with major features are indicated in the figure. This plot shows that for a single simulation, the correlation between the major features and inflow may not be very strong. While Zones GB and GHb both produce close to 10 liters per hour of inflow, Zones GHa and GI produce almost negligible flow. This variability between zones, however, is consistent with known borehole penetrations of this group of zones.

Most prominent in Figure 4-1 is the anomalously high influx at 45 meters, produced by a highly conductive fracture that intersected all of the D-holes. The highest flux from this fracture is into D4. This indicates that the head in this fracture increases with distance upward and southward from the simulated drift. The direction of the gradient indicates that the simulated fracture at 45 meters may be a large, highly transmissive fracture that intercepts one or both of the GH zones. Anomalous features such as this one are to be expected in individual Monte Carlo simulations.

The simulations produced 26 output files containing steady-state nodal flux data of the type shown in Figure 4-1. The results of these Monte Carlo simulations take into account several sources of uncertainty by generating fracture populations from probability distributions. However, the simulations do not take into account uncertainty in the parameters of the transmissivity distributions, or uncertainty in the locations of the major features. These two sources of uncertainty can be accounted for explicitly by appropriate transformations of the flux data.

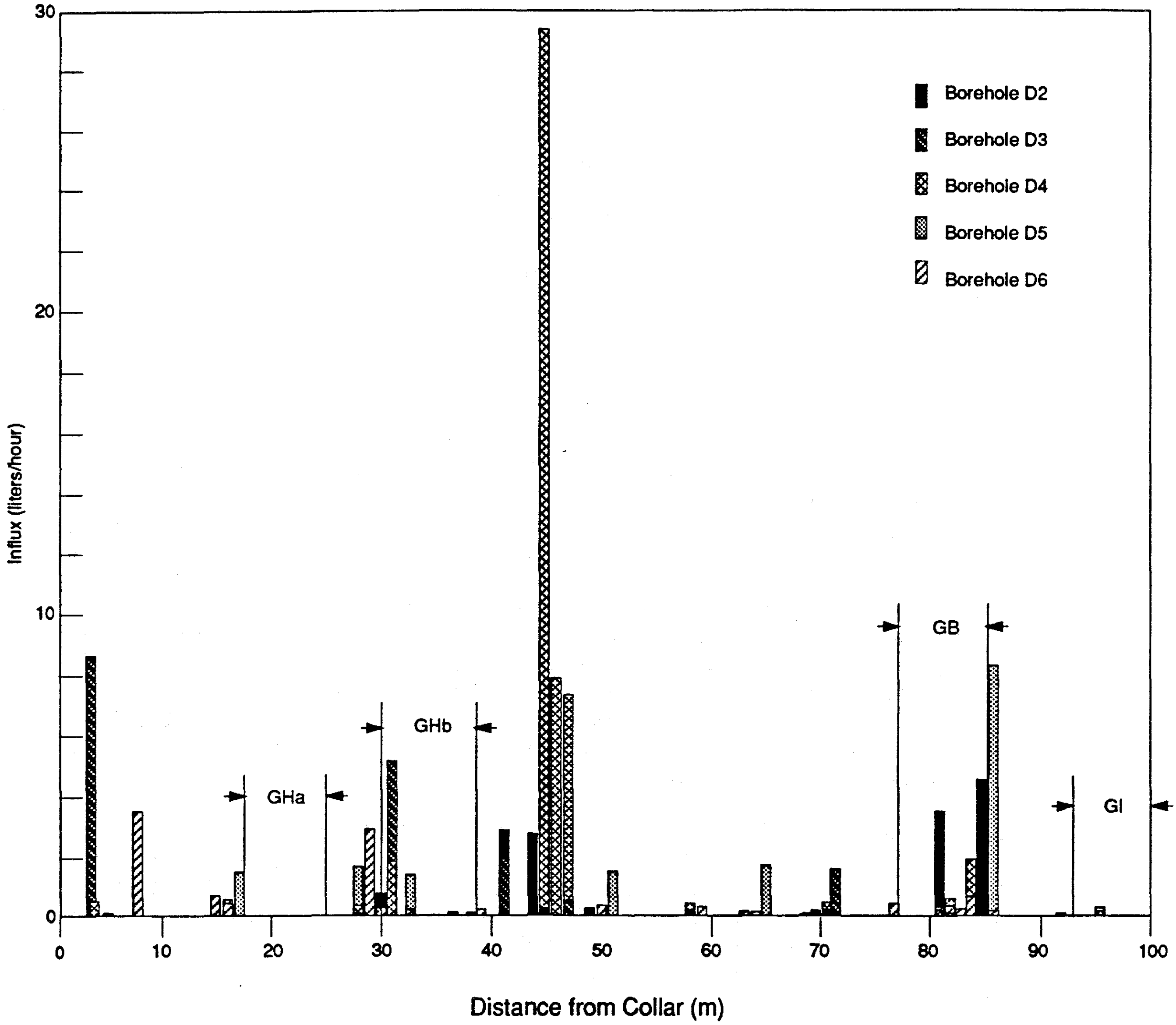

Simulation seed value = 3

Major feature locations shown are those predicted by Olsson et al., 1989.

FIGURE **4-1**
SPATIAL DISTRIBUTION OF FLUX ALONG OUTER D-HOLES FOR A SINGLE SIMULATION
STRIPA

The uncertainty in the means of the transmissivity distributions can be accounted for simply by scaling the predicted fluxes. If the transmissivity of each fracture is expressed as:

$$T_i = \tau_i T_0 \tag{4-1}$$

where

T_i = the transmissivity of the ith fracture,

T_0 = a constant for the fracture system having units of transmissivity, and

τ_i = a dimensionless factor for the ith fracture,

then the steady-state flow equation solved by MAFIC is linear with respect to T_0. If the distribution of transmissivities is taken to be lognormal, then a change $d\mu_{\log T}$ in the logarithmic mean transmissivity of each fracture set is equivalent to multiplying T_0 by a factor:

$$T_0' = T_0 \times 10^{\Delta\mu_{\log T}}. \tag{4-2}$$

Since the predicted flux values are linear with respect to T_0, the effects of a change in $\mu_{\log T}$ can be accounted for by simply scaling the fluxes by the appropriate factor.

Since transmissivity T is lognormally distributed (i.e., log T is normally distributed), by assuming that errors in estimation of $\mu_{\log T}$ are normally distributed, the standard deviation of $\mu_{\log T}$ can be estimated (Benjamin and Cornell, 1970) as:

$$\sigma_{\mu_{\log T}} = \sigma_{\log T}/\sqrt{n} \tag{4-3}$$

where:

n = the number of samples.

Using the derived transmissivity distribution statistics for 7m intervals in the N-holes gives the estimate $\sigma_{\mu_{\log T}} = 0.16$.

This estimate was used to scale the distributions of the flux into each of the D-boreholes, and of the total flux into the D-holes, to account for uncertainty in $\mu_{\log T}$. Uncertainty in the other parameter of the transmissivity distribution, $\sigma_{\log T}$, cannot be accounted for in such a simple fashion. The logarithms of the fluxes in each case were sorted into bins of width 0.05 (log liters/hour) using Lotus 1-2-3. The uncertainty in the logarithmic mean of transmissivity was incorporated by calculating the probability that each binned value belonged in one of the ten bins on either side of the bin to which it had been assigned. The probability of the occurrence of a given flux was estimated as the sum of these probabilities for the bin representing that value of flux. In effect, this was the same as taking a moving, weighted average of the number of flux values in each bin, using a normal probability density function with a standard deviation of $\sigma_{\mu_{\log T}}$ to determine the weights.

The resulting distributions of fluxes in logarithmic space were then transformed back into arithmetic space to obtain the desired probability density functions for flux.

The uncertainty in the locations of fracture zones was accounted for in an analagous manner. The spatial distribution of flux along the D-holes was expected to depend mainly upon the locations of the fracture zones, which were given by Olsson et al. (1989) with estimated confidence intervals of ±4m. The effect of shifting the locations of fracture zones along the D-holes is less unambiguous than the effect of changing the mean transmissivity. However, it is reasonable to assume that shifting the fracture zones a given distance in one direction would, on average, have the effect of shifting the spatial distribution of influx by approximately the same distance.

Since Olsson et al. (1989) gave no indication of the distributional form of the uncertainties in fracture zone locations, it was assumed that the indicated confidence limits represented 90% confidence limits for a normally distributed error in location. The predicted fluxes were sorted into bins for 1m intervals along the D-holes. The uncertainty in location was incorporated by calculating the probability that each binned value belonged in one of the ten bins on either side of the bin to which it had been assigned, and assigning to each bin the product of flux times that probability. The probable flux for each 1m interval was estimated as the sum of these weighted values for flux. In effect, this was the same as taking a moving, weighted average of flux into each 1m interval.

While these corrections for uncertainty in transmissivity distributions and fracture zone locations account for two major sources of uncertainty, it is important to note that only two of many the sources of uncertainty have been dealt with in this manner. Other sources of uncertainty such as uncertainty in the parameters of the fracture radius and orientation distributions have not been accounted for. The effects of errors in these parameters can only be stated qualitatively. For instance, underestimating the log mean of the fracture radius distribution would decrease the connectivity, and thereby decrease both the predicted influx and the predicted number of points where influx occurs; however, the magnitude of these effects cannot be easily estimated.

4.3 D-HOLE FLUX PREDICTIONS

The predictions for the Stripa Phase 3 simulated drift experiment are in the form of probability distributions for inflow quantities and locations. Although the expected values of these distributions are given in the present section, it should be stressed that these predictions are probabilistic in nature and include the possibilities, however remote, of extremely high or low values. In assessing the accuracy of these predictions by comparing them with measured fluxes, the appropriate measures of success must be statistical in nature. The comparisons deemed appropriate by the authors are stated below in the discussions of each part of the prediction.

The first part of the inflow prediction is the distribution of flux into each of the outer D-holes. Figure 4-2 shows the simulated distributions of flux into the D-holes, obtained directly from the Monte Carlo simulations results. Figure 4-3 shows the predicted probability density function for the flux into individual, outer boreholes, obtained by correcting for the uncertainty in the parameters of the transmissivity distribution, as described in Section 4.3. The flux into the inner borehole, D1, is expected to be two or more orders of magnitude less than the flux to the outer boreholes; this explains the high probability density for very low inflows shown in Figure 4.2.

In assessing the accuracy of this prediction, the quantitative values should be of less concern than the observable patterns in the flux distributions. The comparison of measured and predicted distributions of flux among boreholes should be based upon relative differences in flux to different boreholes. That is, the standardized (with respect to the mean) variance of flux among boreholes should be approximately the same as for the predicted distribution of flux, although the magnitudes may not necessarily be the same.

Figure 4-4 gives the simulated probability distribution for the total flux into all D-holes. Figure 4-5 gives the predicted probability distribution for the quantity, obtained by correcting for uncertainty in the parameters of the transmissivity distribution as described in Section 4.3. The mean value of this distribution is 90 liters/hour. The 90 percent confidence interval for the total flux is between 30 and 5700 liters/hour. The basis for the comparison of the measured influx with the predicted flux distribution should be a calculation of the confidence level for accepting the hypothesis that the measured flux belongs to the predicted distribution.

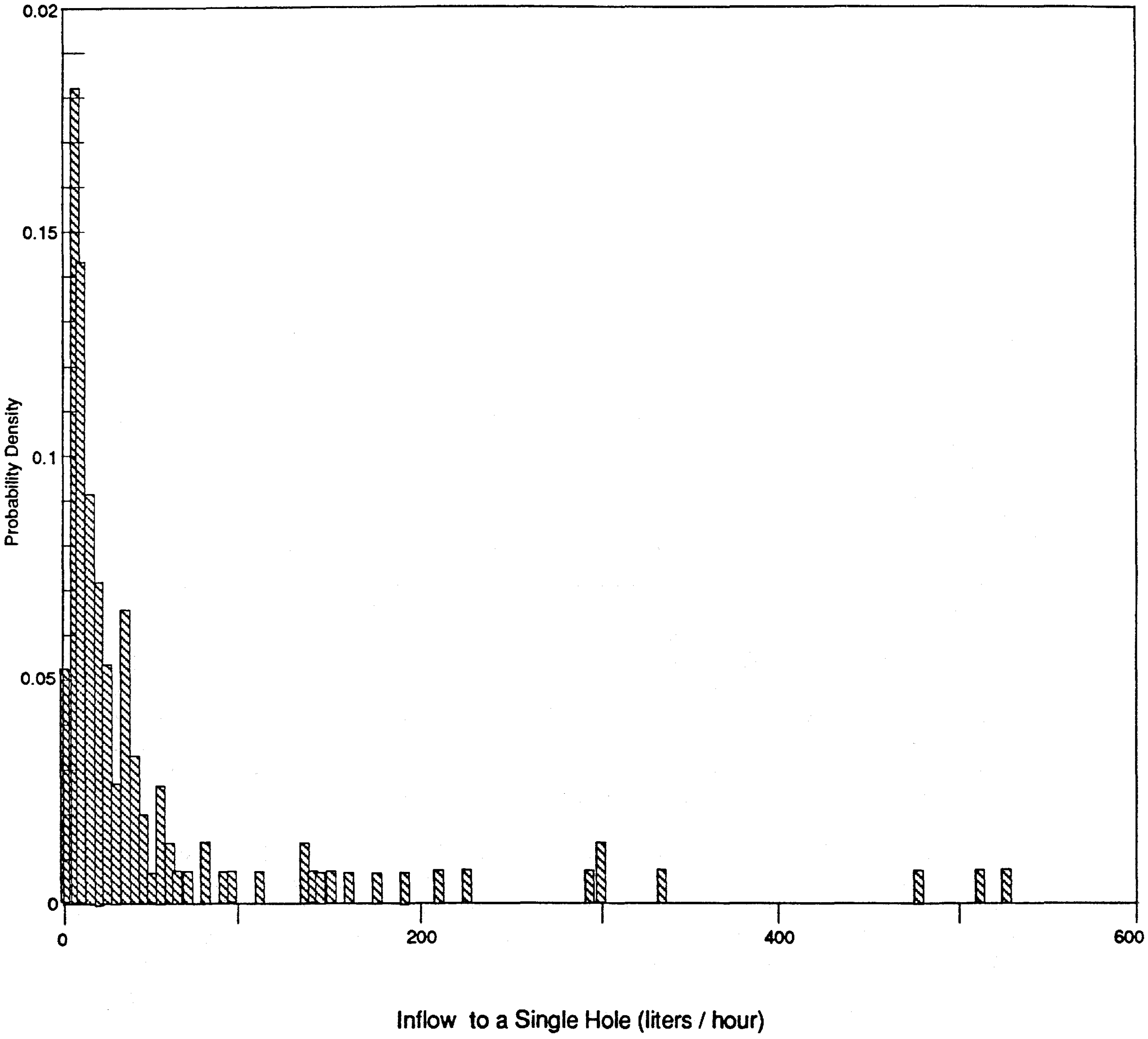

FIGURE **4-2**

SIMULATED DISTRIBUTION OF FLUX TO D-HOLES

STRIPA

PROJECT NO. 883-1313.220 DWG. NO. 22067 DATE 4/12/90 DRAWN CB

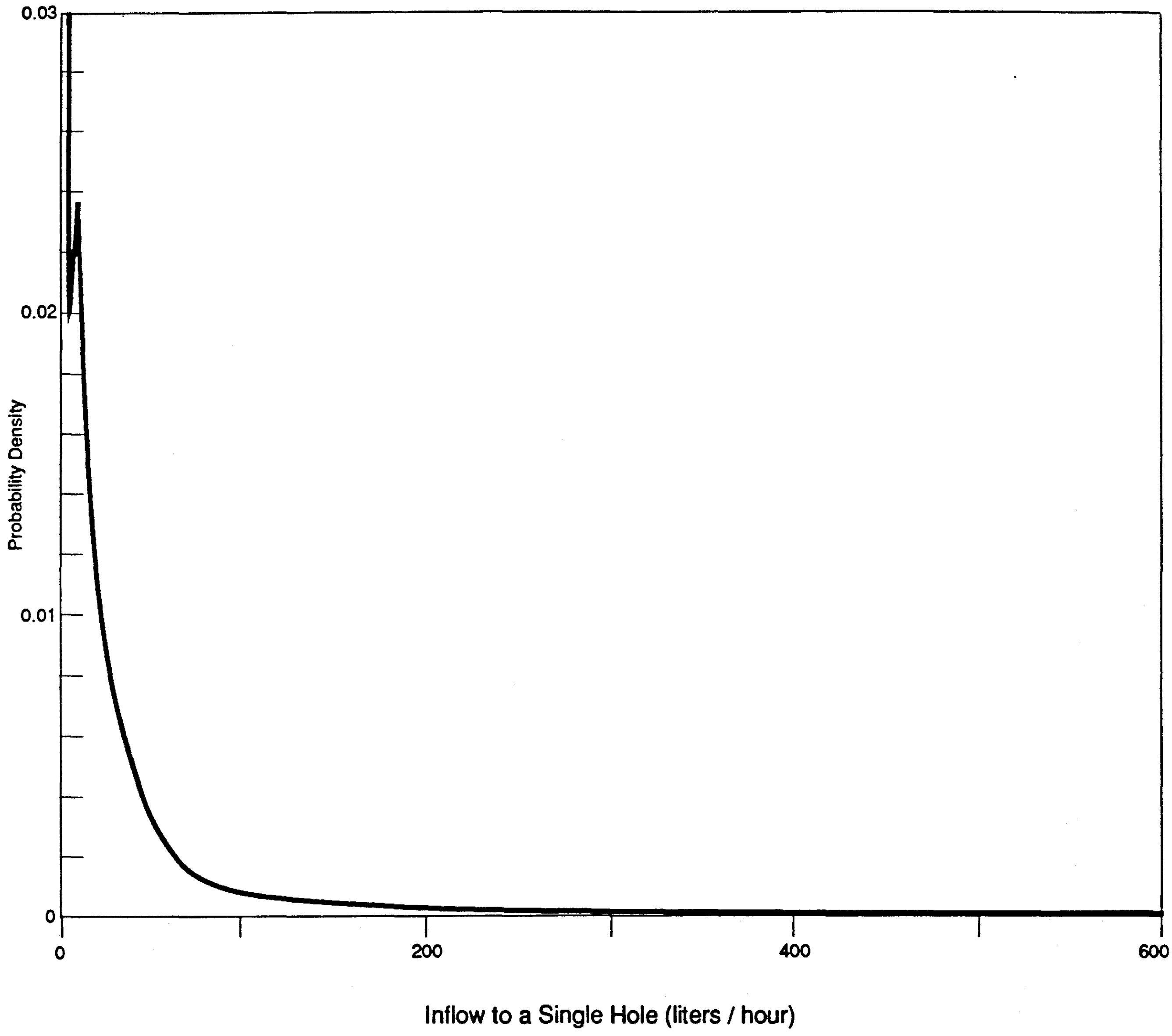

FIGURE **4-3**
PREDICTED DISTRIBUTION OF FLUX TO D-HOLES
STRIPA

PROJECT NO. 883-1313.220 DWG. NO. 22066 DATE 4/12/90 DRAWN CB

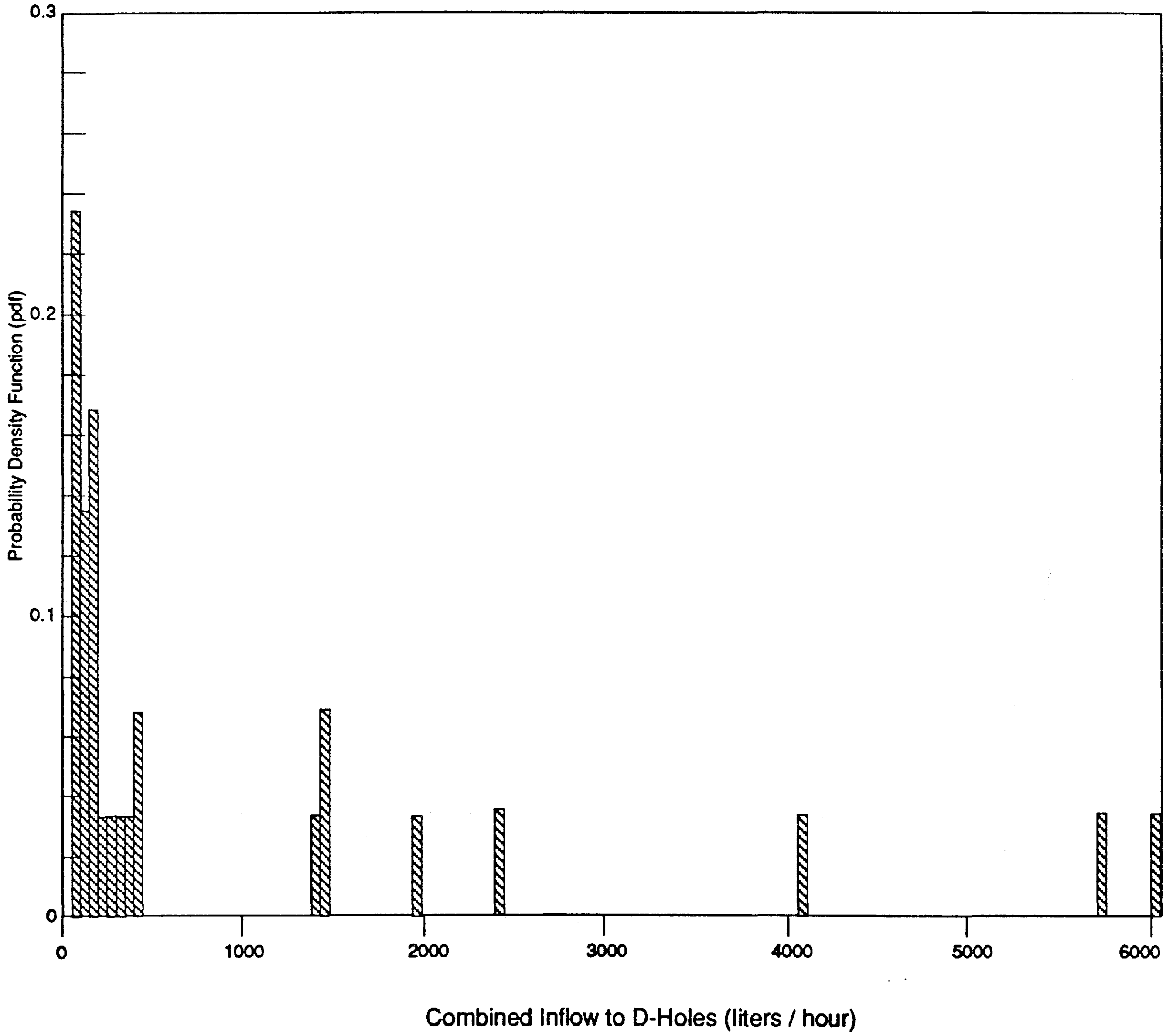

FIGURE **4-4**
SIMULATED DISTRIBUTION OF TOTAL FLUX INTO D-HOLES
STRIPA

PROJECT NO. 883-1313.220 DWG. NO. 00000 DATE 4/10/89 DRAWN CB

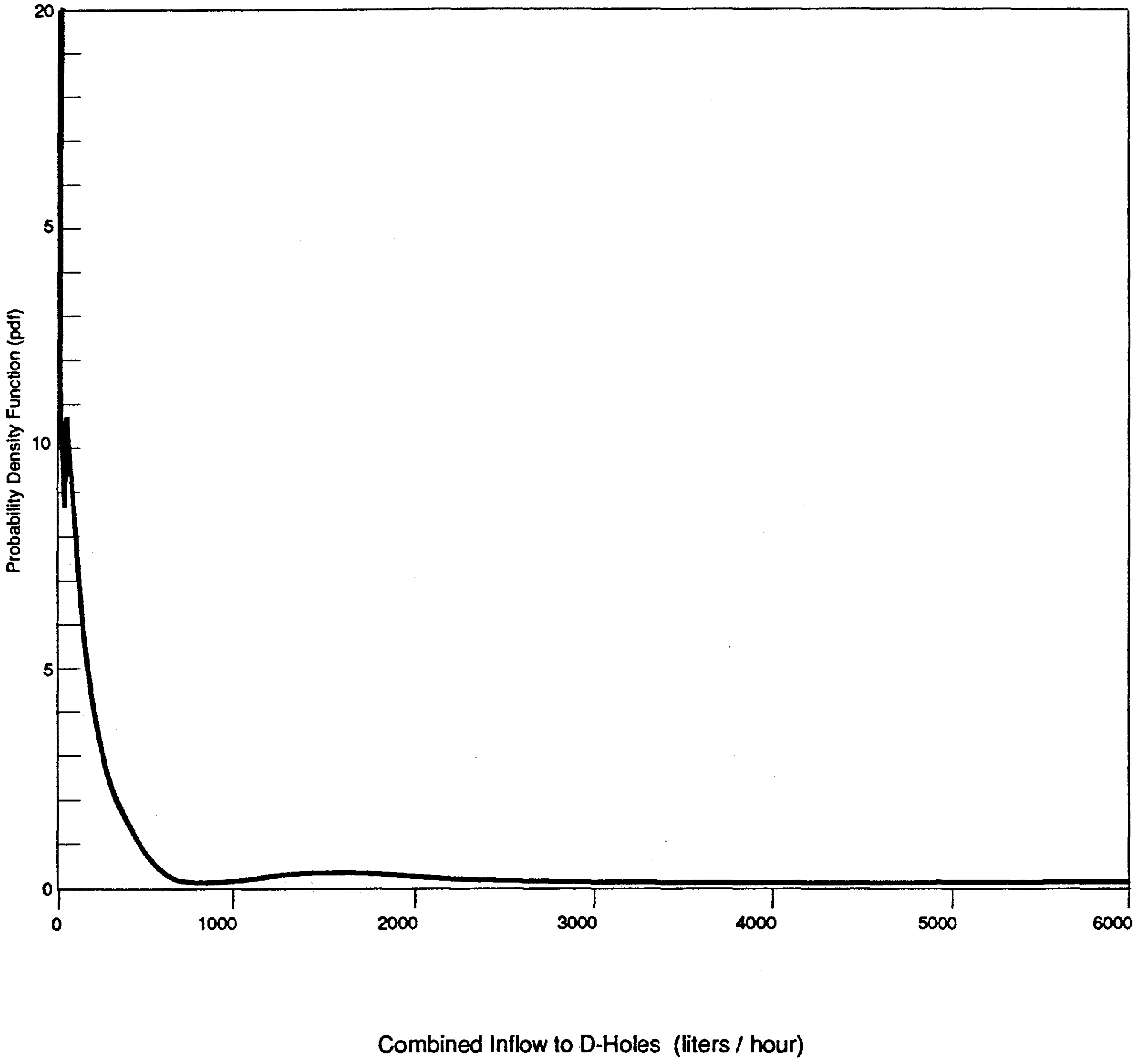

FIGURE **4-5**
PREDICTED DISTRIBUTION OF TOTAL FLUX INTO D-HOLES
STRIPA

PROJECT NO. 883-1313.220 DWG. NO. 22062 DATE 4/12/90 DRAWN CB

Figure 4-6 gives the simulated spatial distribution of flux along the D-holes. Figure 4-7 gives the predicted distribution of flux along the D-holes, obtained by correcting for uncertainty in the location of the major features (but not uncertainty in the mean of the transmissivity distribution) as described in Section 4.3. Fracture zones are shown in the locations predicted by Olsson et al., 1989. The fracture zones in this plot are generally in or close to zones of elevated influx, except for Zone GI. Figure 4-8 shows the simulated distribution of flux into 1 m intervals, which shows the high proportion of intervals with very little flow.

In Figure 4-7, the predicted values of flux slightly uphole of the major zones are generally higher than in the fracture zones themselves. In part this can be attributed to a bias in the averaging method used, in which a few simulatons that produced very high fluxes had a dominating influence on the form of the predicted flux distribution. Another way of viewing the results is to normalize the fluxes in terms of the total flux for each run, and to present the results as a distribution of the percentage of influx in each 1m interval (Figure 4-9). In this figure, the predominance of the results from high-flux simulations is diminished.

However, these results still indicate that there is a high probability of high-flow zones occurring slightly uphole of the major features. This is an expected result of the War Zone conceptual model, in which the major fractures associated with a fracture zone are not necessarily parallel to the fracture zone. Large fractures connected to a fracture zone will tend to intersect the D-holes at a distance from the fracture zone which is determined by the preferred orientation and size of the large fractures. The ability of the model to predict the likelihood of high fluxes outside of the identified fracture zones is a unique feature of discrete-fracture models.

The accuracy of the predicted flux distribution should be assessed qualitatively rather than quantitatively, by comparing patterns in the predictions with patterns in the measured flux distributions. The spatial correlation of the influx, the proportion of the total influx accounted for by fracture zones, and the variability among fracture zones should be similar in the predicted and the measured flux distributions. Figure 4-10 shows a variogram of the normalized flux distribution, which gives the expected structure of spatial correlation for flux to the D-holes. The variogram shows the average square of the difference in flux values measured at different points along the D-holes, plotted as a function of distance between the measurement points.

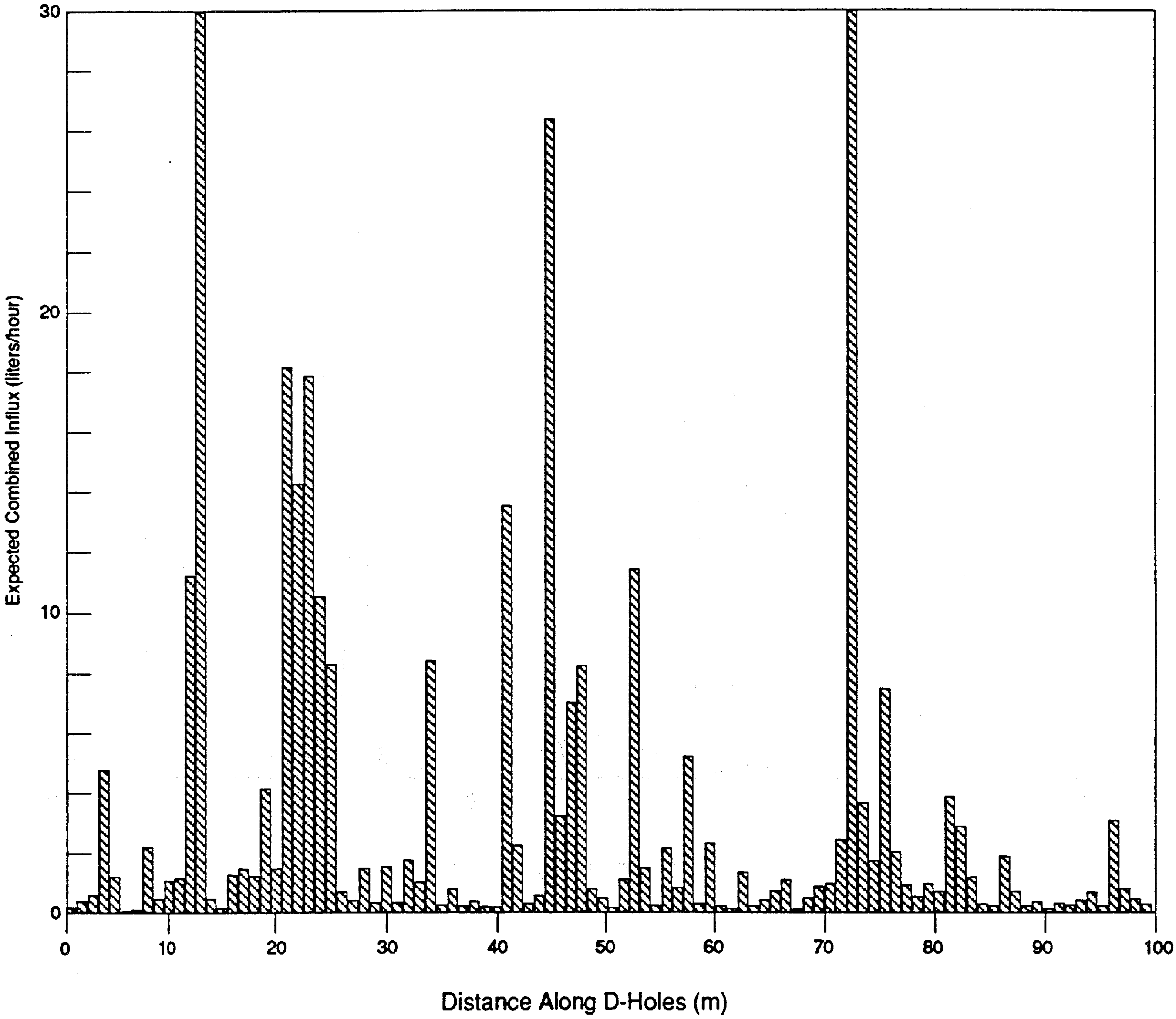

FIGURE **4-6**
SIMULATED SPATIAL DISTRIBUTION OF FLUX INTO THE D-HOLES
STRIPA

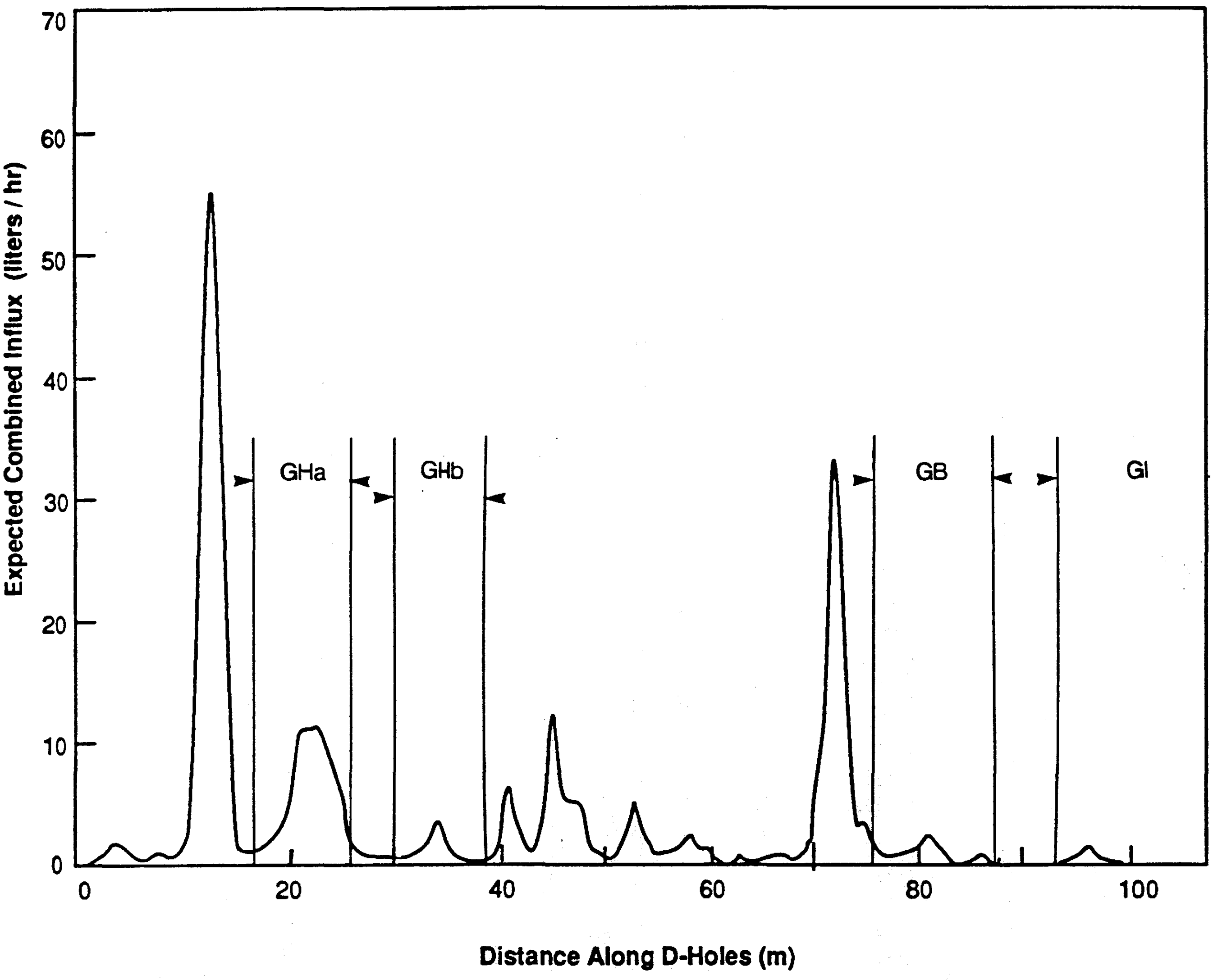

FIGURE **4-7**

PREDICTED SPATIAL DISTRIBUTION OF FLUX INTO D-HOLES

STRIPA

PROJECT NO. 0883-1313.031 DWG. NO22080 DATE 4/27/90 DRAWN DC

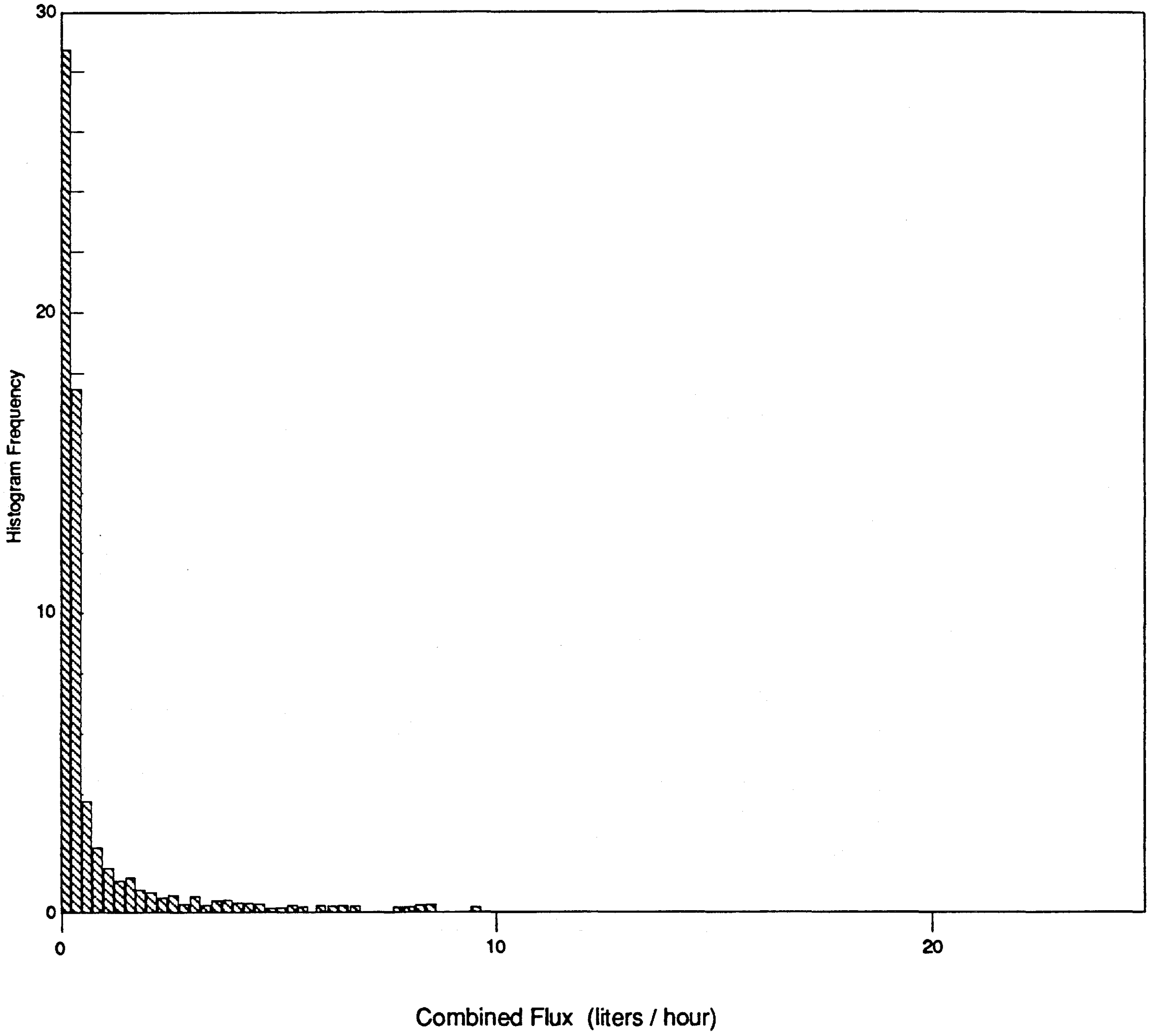

FIGURE **4-8**
SIMULATED DISTRIBUTION OF FLUX INTO 1 m INTERVALS ALONG D-HOLES
STRIPA

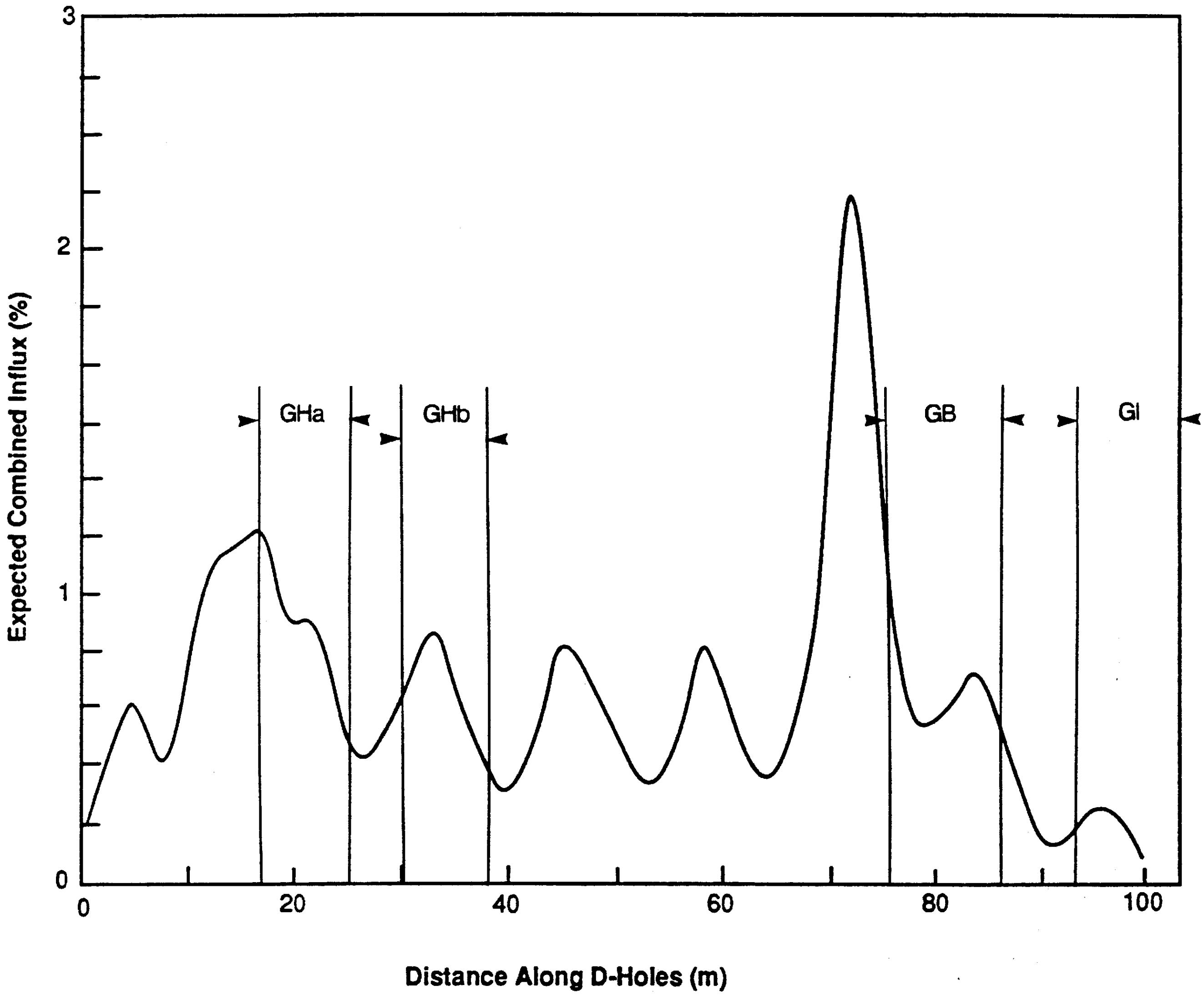

FIGURE **4-9**

SPATIAL DISTRIBUTION OF FLUX INTO D-HOLES AS PERCENTAGE OF TOTAL FLUX

STRIPA

PROJECT NO. 83-1313.031 DWG. NO. 22078 DATE 4/27/90 DRAWN DC

The flux along the borehole can be treated as a stationary, stochastic process with respect to location, and be described in terms of the mean, standard deviation, and autocorrelation of values of flux to 1m intervals. These statistics can be calculated for the simulated and observed spatial distributions of flux, and used as a basis for comparison. For the simulated distributions, it is possible to calculate the variability of these statistics as well, since one value of each statistic is obtained from each distribution. Table 4-3 gives statistics describing the variability of the mean and standard deviation of flux within 1m intervals. The autocorrelation statistics were not calculated, but can be estimated from Figure 4-10. The variability of the equivalent statistics on a logarithmic scale is also given.

Table 4-3. Variability of Mean and Standard Deviation of Flux to 1m Intervals along D-Holes

Statistics	Mean of Statistics	Standard Deviation of Statistic	
Mean Flux	9.0	13.5	(1/hr)
Standard Deviation of Flux	60.8	110.1	(1/hr)
Standardized Standard Deviation of Flux	4.9	2.0	(-)
Mean Log Flux	-2.28	0.44	(log 1/hr)
Standard Deviation of Log Flux	1.91	0.26	(log 1/hr)
Standardized Standard Deviation of Log Flux	0.89	0.29	(-)

Due to time constraints, only steady-state responses were modeled. A prediction of the transient flux into the D-holes was therefore not obtained.

4.4 COMMENTS ON THE MODELING APPROACH

This prediction exercise was the first full-scale implementation of recently developed software. The process of installing and running this code on a mainframe computer provided invaluable experience with regard to limits on the size and type of fracture network problems that are practicable. The number of simulations that could be completed was limited due to problems associated with the transferral of the large fracture population datasets from personal computers to the mainframe computer that was used to generate meshes and run MAFIC.

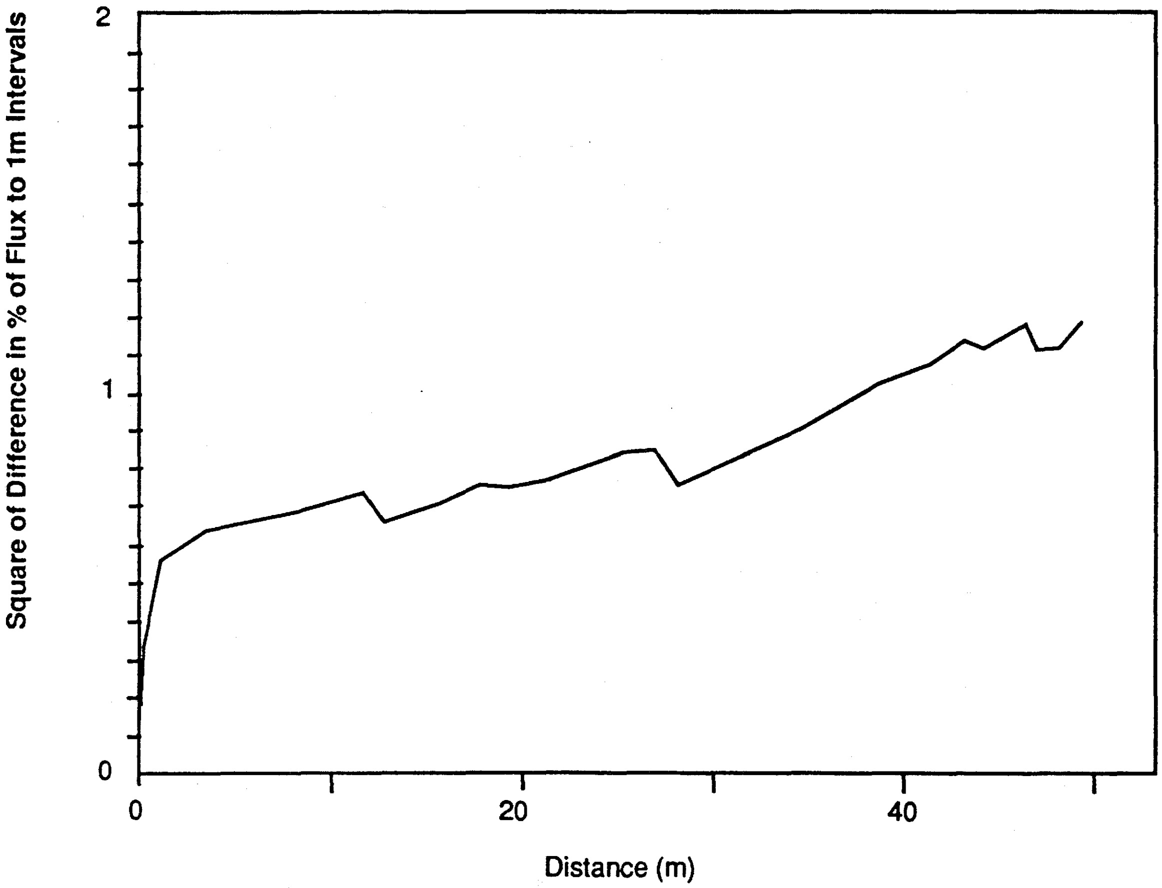

FIGURE **4-10**

PREDICTED VARIOGRAM OF NORMALIZED FLUX INTO 1m INTERVALS ALONG D-HOLES

STRIPA

PROJECT NO. 883-1313.031 DWG. NO. 22079 DATE 4/27/90 DRAWN DC

The work was further hindered by need for numerous trial-and-error refinements that were necessary to develop a workable dataset. Because connectivity was the most important determinant of the feasibility of modeling fracture systems, and because reliable rules-of-thumb were not available for predicting connectivities from more easily controlled fracture statistics, the process of fitting the problem to the computer was very difficult. One positive aspect of these struggles was the development of a database relating fracture network parameters to mesh size and feasibility. This information will be extremely useful for the next modeling task of the Phase 3 program, the prediction of inflows to the validation drift.

This modeling effort revealed a problematic aspect of finite element networks generated by FracMan for solution by MAFIC. The presence of isolated groups of fractures that were not connected to any boundary resulted in ill-posed matrix equations that produced instabilities in the MAFIC matrix solver. In a preliminary attempt at modeling the SDE inflows, 24 out of 30 fracture populations resulted in ill-posed meshes of this type. Further work on the Fracman mesh generator was needed to eliminate these fracture groups (which do not contribute to flow) from the meshes before running MAFIC. This work was successfully accomplished, and no ill-posed problems were encountered in the final round of runs for this prediction exercise.

4.5 CRITICAL PARAMETERS FOR FRACTURE FLOW MODELING

The critical parameters for fracture flow modeling are those which control:

- the verisimilitude of the model, and
- the feasibility of implementing the model.

The verisimilitude of the model is the degree to which the hydrological properties of the modeled system reflect the properties of the real fracture system. This is controlled primarily by the connectivity of the fracture system, since the existence or nonexistence of a flow path between two given points is the primary hydrological characteristic of the system with regard to those two points.

Connectivity depends upon the aggregate of several geometric characteristics of the fracture system, including

- fracture intensity,
- fracture size distribution, and
- fracture orientation.

Fracture intensity or, more specifically, the spatial distribution of fracture intensity is arguably the primary determinant of connectivity, although size distribution and orientation can in certain cases be dominant. For example, if all fractures are parallel and small relative to the scale of the model, the connectivity will be very low even if the fracture intensity is extremely high. However, when several sets of fractures with contrasting orientations are present, the connectivity of the model will be relatively insensitive to the parameters of the orientation distributions (Dershowitz, 1984; Dershowitz and Einstein, 1988).

If one or more flow paths exist, the cross-fracture transmissivities of the fractures, and the transmissivities of fracture intersections in those flow paths are critical. Since the transmissivity of the least conductive elements in a flow path control the flux, the distribution of transmissivities (not just the mean transmissivities) has a strong influence on flux. For transient flow and solute transport calculations, the storativity and diffusivity of fractures and fracture intersections are also critical.

The feasibility of implementing the model is controlled by several parameters that determine the amount of computer memory, disk storage, and CPU time needed to simulate flow through fracture systems. Probabilistic modeling of fracture systems consists of three stages, each of which is controlled by specific critical parameters:

- **Monte Carlo simulations of fracture properties and geometries (FracMan)**: The CPU time required for FracMan simulations, and the amount of disk storage and RAM memory are controlled primarily by the number of fractures, and only indirectly by the fracture intensity P_{32}. Generation of 10,000 standard Baecher fractures requires only approximately 5 minutes of CPU time and 1.5 Meg hard disk space on a 386 PC. Time and storage requirements are linear, such that 100,000 fractures would require 1 hour, and 1,000,000 fractures 10 hours. However, due to the integer precision in the current code, a maximum of 32,798 fractures can be generated in a single simulation.

  The second most important constraint on CPU time is the degree of sophistication of the conceptual model used for fractures. Due to requirements for searching through existing fractures for generation of subsequent fractures, the CPU time requirement of the Enhanced Baecher Model, Nearest Neighbor Model, and Fractal (Levy-Lee) models increases with the square of the number of fractures. 1,000 and 10,000 fractures for these models takes approximately 0.5 and 5 hours, respectively on a 386 PC. In the standard (stochastic) war zone model, the identification of war zones can be very computationally intensive if the number of fractures in the set forming war zones is greater than approximately 1,000. The deterministic war zone model utilized in this study requires approximately 30 percent more CPU time than the standard Baecher model.

- Mesh Generation (Meshmaker): The CPU time for mesh generation depends linearly upon the number of fractures, and non-linearly upon the maximum and average number of intersections per fracture. As a result, mesh generation is extremely sensitive to network connectivity. For many fracture systems, mesh generation is more sensitive to network connectivity than to the number of fractures. CPU time for 10,000 fractures with an average of 3 intersections per fracture is 1.5 hours on a VAX 8600, increasing to 16 hours with an average of 20 intersections per fracture. As discussed above, network connectivity is a function of fracture intensity, size, and orientation distributions.

- Finite Element Flow Solution (MAFIC): The CPU time for MAFIC varies approximately linearly with the average bandwidth and the number of fractures. Bandwidth depends directly upon fracture network connectivity, and can increase non-linearly for high connectivities. Hence, connectivity is the most important factor in determining MAFIC solution time. The number of fractures depends upon a combination of the number of fractures included in the fracture network, and cutoffs established on minimum fracture transmissivity. The number of iterations required for solution convergence depends upon the convergence tolerance and the variability of fracture transmissivity and storativity.

In summary, both the verisimilitude and feasibility of discrete fracture models are directly dependent upon fracture connectivity and the number of fractures. Connectivity, in turn, is dependent upon fracture intensity, size, and orientation distribution, while the number of fractures is dependent upon fracture intensity, and fracture transmissivity cutoffs defined for simulations. In these simulations, the number of fractures included in the model, and the sophistication of the fracture geometric conceptual model, were established at a level sufficient to allow Monte Carlo simulation.

5 CONCLUSIONS

This report described discrete fracture flow modeling performed by Golder Associates Inc. as part of the Site Characterization and Validation (SCV) Project, within Phase 3 of the Stripa Project. This modeling predicted flow into the simulated drift experiment, as a rehearsal for modeling of flow into the SCV drift during 1990. The influx predictions developed express the uncertainty inherent in the hydrologic behavior of geologic systems, and are not substantially different from predictions which could be made directly from existing data on distributions of borehole and drift pressures and inflows on the SCV site. The predictions developed in the present study are, of course, more significant than simple predictions of flux based on observed fluxes, because the model can be extended to predict other aspects of behavior of flow through fractures at the site. Validation of model predictions will depend upon the degree to which the predictions made correspond to those observed in the simulated drift experiment. The real value of the exercise, however, lies in development and demonstration of all of the components necessary for practical applications of discrete fracture flow modeling.

The simulated drift prediction exercise demonstrated that the data necessary for discrete fracture modeling can be collected within the scope of a standard site characterization program, as well as the application and importance of different types of data. It also demonstrated the new, probabilistic data-analysis techniques necessary to convert field data into the form necessary for modeling. Producing this prediction with the PC- and VAX-based FracMan/MAFIC codes demonstrated that meaningful, discrete-fracture modelling can be carried out with ordinary computing resources.

Having shown the possibility of practical application of discrete fracture methods through this prediction exercise, the next stage of the Stripa project will require refinement of field data, data analysis techniques, conceptual models, and improvement in efficiency and capabilities of discrete fracture modeling software. The application of fracture-flow modeling to future stages of the SCV project will complete the evolution of this method from a research topic to a practical technique for repository design.

6 ACKNOWLEDGEMENTS

The modeling work described in this report was supported by the United States Department of Energy, through a contract managed by the Office of Waste Technology Development, Battelle Memorial Institute. The authors wish to extend their special thanks to Dr. Levy Kroitoru, for his technical direction, and to Ms. Sharon Steidl, who has been extremely generous in helping the authors run fracture-flow codes on the OWTD VAX. The authors also wish to thank Dr. Glori Lee of Golder Associates for her invaluable efforts toward improving the FracMan code, and Dr. Charles Wilson and Dr. Thomas Doe for their excellent review comments.

7 REFERENCES

Benjamin, J.R. and C.A. Cornell, 1970. Probability, Statistics, and Decision for Civil Engineers, McGraw-Hill Book Company, New York, USA.

Carlsten, S., O. Olsson, O. Persson, M. Sehlstedt, 1988. "Site Characterization and Validation-Monitoring of Head in the Stripa Mine During 1987," Stripa Project Technical Report 88-02.

Cheeney, R.F., 1983. Statistical Methods in Geology, George Allen & Unwih, London, UK.

Dershowitz, W. S., 1985. "Rock Joint Systems," PhD dissertation, Massachusetts Institute of Technology, Cambridge, Massachusetts, USA.

Dershowitz, W.S. and H.H. Einstein, 1988. "Characterizing Rock Joint Geometry with Joint System Models," Rock Mechanics and Rock Engineering, Vol. 21, pp. 21-51.

Feller, W., 1971. An Introduction to Probability Theory and its Applications, John Wiley and Sons, New York, USA.

Gale, J., 1989. Stripa Project memorandum dated February 14, 1989.

Gale, J., and A. Strahle, 1988. "Site Characterization and Validation--Drift and Borehole Fracture Data Stage I," Stripa Technical Project Report 88-10.

Gale, J., R. MacLeod, J. Welhan, C. Cole, and L. Vail, 1987. "Hydrogeological Characterization of the Stripa Site," Stripa Project Technical Report 97-15.

Geier, J.E., K. Lee, and. W.S. Dershowitz, 1988. "Field Validation of Conceptual Models for Fracture Geometry," paper H12A-11 presented at the American Geophysical Union 1988 Fall Meeting.

Golder Associates Inc., 1988a. "Stripa Phase III Preliminary Flow Validation Prediction," prepared for Battelle Office of Waste Technology Development, Willowbrook, Illinois, USA.

Golder Associates Inc., 1988b. "FracMan Version 2.0 Interactive Rock Fracture Geometric Model: User Documentation," prepared for Battelle Office of Waste Technology Development, Willowbrook, Illinois, USA.

Golder Associates Inc., 1988c. "MAFIC/T Version 1.0 Matrix/Fracture Interaction Code with Solute Transport User Documentation," prepared for Battelle Office of Waste Technology Development, Willowbrook, Illinois, USA.

Jaeger and Cook, 1977. Fundamentals of Rock Mechanics, 2nd edition, Halsted Press, New York, New York, USA.

Kenrick, M.P., P.J. Fennessy, and G. Sharp, 1989. "Hydrologic Testing of Channelized Rock Fractures; A Numerical Simulation," report prepared for Battelle Office of Waste Technology Development by Golder Associates Inc., Redmond, Washington, USA.

Olsson, O., J.H. Black, J.E. Gale, D.C. Holmes, 1989. "Site Characterization and Validation Stage 2-Preliminary Predictions," Stripa Project IR 89-03, SGAB, Uppsala, Sweden.

Osnes, J.D., A. Winberg, and J. Andersson, 1988. "Analysis of Well Test Data -- Application of Probabilistic Models to Infer Hydraulic Properties of Fractures," Topical Report RSI-0338, RE/SPEC Inc., Rapid City, South Dakota, USA.

Patrick, G., 1989. "Preliminary data from crosshole tests in the N- and W-holes at the Stripa mine," memorandum to T. Doe July 19, 1989, Golder Associates Inc., Redmond, Washington, USA.

Terzaghi, R., 1965. "Sources of error in joint surveys," Geotechnique, Vol. 15, pp. 287-304.

Thorpe, R., 1979. "Characterization of Discontinuities in the Stripa Granite Time-Scale Heater Experiment," Lawrence Berkeley Laboratory Report LBL-7083, SAC-20. Berkeley, California, USA.

Wikberg, P., M. Laaksoharju, J. Bruno, and A. Sandino, 1988. "Site Characterization and Validation - Hydrochemical Investigations in Stage I," Stripa Technical Project Report 88-09.

8 NOTATION

A_i - area of the ith fracture

f - fracture frequency (number per unit length)

f_c - conductive fracture frequency

f_o - fracture frequency outside of fracture zones

f_w - fracture frequency within fracture zones

g - ratio of fracture frequency to fracture intensity - f/P_{32}

H_o - value head at the origin (0,0,0)

H_x - coefficient of head variation with respect to x

H_y - coefficient of head variation with respect to y

H_z - coefficient of head variation with respect to z

K - Fisher dispersion parameter

k_i - weighting factor for ith fracture set used by ISIS

L - trace length

L_t - total length of boreholes

L_w - length of boreholes inside fracture zones

L_o - length of boreholes outside fracture zones

m_T - scaling factor for fracture transmissivity

n - exponent of transmissivity/stress relationship

$\bar{n}$ - mean number of conductive fractures within a test zone

N - number of fractures

N_c - number of conductive fractures

n_i - number of conductive fractures within the ith test zone

p_1 - maximum far-field stress

p_2 - minimum far-field stress

P_{32} - fracture intensity (area per unit volume)

P_{32c} - conductive fracture intensity

P_{32co} - conductive fracture intensity outside of war zones

P_{32cw} - conductive fracture intensity inside of war zones

Q_{mi} - flux measured at the ith measurement point

Q_{pi} - flux predicted at the ith measurement point

V_w - total volume of war zones

r - radial distance or fracture radius

R - radius of a borehole or drift

T - transmissivity of a fracture

T_{1MPa} - transmissivity of a fracture at 1 MPa normal stress

T_i - transmissivity of the ith test zone

T_{ij} - transmissivity of the jth fracture in the ith test zone

T'_{ij} - observed transmissivity of the jth fracture in the ith test zone

V - volume of the modeling region

w - weighting factor

x - southward in the FracMan coordinate system

y - eastward in the FracMan coordinate system

z - upward in the FracMan coordinate system

α - angle between a fracture pole and the normal to a traceplane

β - angle between a fracture pole and a borehole or scanline

θ - azimuth of a dip or pole vector

$\mu_{\ln L}$ - mean of ln L

$\mu_{\ln r}$ - mean of ln r

$\mu_{\log T}$ - mean of log T_{ij}

ϕ	= inclination of a dip or pole vector
ρ	= r/R
σ	= normal stress
$\sigma_{\ln L}$	= standard deviation of ln L
$\sigma_{\ln r}$	= standard deviation of ln r
$\sigma_{\log T}$	= standard deviation of log T_{ij}
σ_r	= radial component of stress
σ_θ	= tangential component of stress